



Akt regulates skeletal development through GSK3, mTOR, and FoxOs

Satoshi Rokutanda^{a,b}, Takashi Fujita^a, Naoko Kanatani^a, Carolina A. Yoshida^a, Hisato Komori^a, Wenguang Liu^a, Akio Mizuno^b, Toshihisa Komori^{a,*}

^a Department of Cell Biology, Unit of Basic Medical Sciences, Nagasaki University Graduate School of Biomedical Sciences, 1-7-1 Sakamoto, Nagasaki 852-8588, Japan

^b Department of Oral and Maxillofacial Surgery, Unit of Translational Medicine, Nagasaki University Graduate School of Biomedical Sciences, 1-7-1 Sakamoto, Nagasaki 852-8588, Japan

ARTICLE INFO

Article history:

Received for publication 4 September 2008

Revised 24 December 2008

Accepted 6 January 2009

Available online 14 January 2009

Keywords:

Akt
GSK3
mTOR
FoxO
Chondrocyte maturation
Chondrocyte proliferation
Cartilage matrix
Cell growth
Transgenic mouse
Skeletal development

ABSTRACT

Although Akt plays key roles in various cellular processes, the functions of Akt and Akt downstream signaling pathways in the cellular processes of skeletal development remain to be clarified. By analyzing transgenic embryos that expressed constitutively active Akt (myrAkt) or dominant-negative Akt in chondrocytes, we found that Akt positively regulated the four processes of chondrocyte maturation, chondrocyte proliferation, cartilage matrix production, and cell growth in skeletal development. As phosphorylation of GSK3 β , S6K, and FoxO3a was enhanced in the growth plates of myrAkt transgenic mice, we examined the Akt downstream signaling pathways by organ culture. The Akt-mTOR pathway was responsible for positive regulation of the four cellular processes. The Akt-FoxO pathway enhanced chondrocyte proliferation but inhibited chondrocyte maturation and cartilage matrix production, while the Akt-GSK3 pathway negatively regulated three of the cellular processes in limb skeletons but not in vertebrae due to less GSK3 expression in vertebrae. These findings indicate that Akt positively regulates the cellular processes of skeletal growth and endochondral ossification, that the Akt-mTOR, Akt-FoxO, and Akt-GSK3 pathways positively or negatively regulate the cellular processes, and that Akt exerts its function in skeletal development by tuning the three pathways in a manner dependent on the skeletal part.

© 2009 Elsevier Inc. All rights reserved.

Introduction

Endochondral ossification, a process involving a cartilage intermediate, is responsible for the formation of most vertebrate skeletal elements including the chondrocranium, vertebral column, ribs, scapulae, pelvis, and limb bones (DeLise et al., 2000). After condensation of mesenchymal chondroprogenitor cells, cells differentiate into chondrocytes, which express cartilaginous matrix molecules and form cartilage that prefigures future skeletal elements. Endochondral bone growth takes place at the growth plate, where chondrocytes undergo unidirectional proliferation and then mature to become hypertrophic chondrocytes. Hypertrophic chondrocytes eventually undergo apoptosis and are replaced by bone cells (Nakashima and de Crombrughe, 2003).

Akt/protein kinase B (PKB), which belongs to the family of serine/threonine protein kinases, has been highly conserved throughout evolution (Datta et al., 1999). Akt1 and Akt2 share extensive sequence homology at the amino acid level, whereas Akt3 is slightly more divergent in structure and is expressed as a splice variant that lacks a regulatory phosphorylation site (Brodbeck et al., 2001). Akt protein kinases are stimulated by a number of receptor tyrosine kinases and G

protein-coupled receptors (Kandel and Hay, 1999; Brazil and Hemmings, 2001; Lawlor and Alessi, 2001) through phosphatidylinositol 3-kinase (PI3K) (Cantley, 2002). The lipid product of PI3K, PIP3 (phosphatidylinositol 3,4,5 triphosphate), recruits both PDK1 and Akt to the plasma membrane. Akt is subsequently phosphorylated on T308 by PDK1 and on S473 by mTORC2 (consisting of mTOR, mLST8, and Rictor), leading to full activation (Sarbasov et al., 2005; Corradetti and Guan, 2006).

Insulin-like growth factor (IGF) is an anabolic growth factor required for fetal and postnatal development, and IGF signaling regulates both embryonic and postnatal body/organ size, as evidenced by general growth retardation of *Igf1*- or *Igf1r*-deficient mice (Baker et al., 1993; Liu et al., 1993; Powell-Braxton et al., 1993). Most of the circulating IGF-I is produced by the liver and transported to other tissues, acting as an endocrine hormone. IGF-I is also produced by many tissues, including bone cells and chondrocytes, and acts locally as an autocrine/paracrine hormone (Le Roith et al., 2001). Genetic approaches revealed that the IGFs-IGF receptor-PI3K-Akt pathway plays key roles in skeletal growth and endochondral ossification. *Igf1*-deficient mice, *Igf1r*-deficient mice, and *Akt1/Akt2*-deficient mice showed retarded skeletal growth and endochondral ossification, while conditional *Pten*-deficient mice showed accelerated skeletal growth and chondrocyte maturation (Baker et al., 1993; Liu et al., 1993; Powell-Braxton et al., 1993; Peng et al., 2003; Wang et al., 2006; Ford-Hutchinson et al., 2007).

Akt activates or inhibits many molecules including GSK3, TSC2, FoxOs, BAD, MDM2, Caspase 9, AS160, eNOS, and PRAS40 by phos-

Abbreviations: myrAkt, myristoylated Akt; EGFP, enhanced green fluorescence protein; tg(L), transgenic mice with low expression; tg(H), transgenic mice with high expression; FoxO3a-TM, FoxO3a triple mutant; dn, dominant negative.

* Corresponding author. Fax: +81 95 819 7633.

E-mail address: komorit@nagasaki-u.ac.jp (T. Komori).

phorylation, leading to the regulation of various cellular processes such as metabolism, growth, differentiation, proliferation, survival, glucose uptake, and angiogenesis. Akt regulates the activities of three FoxO proteins, FoxO1/FKHR, FoxO3a/FKHRL1, and FoxO4/AFX (Brunet et al., 1999), which have overlapping patterns of expression and transcriptional activities (Anderson et al., 1998; Furuyama et al., 2000). Following activation by PI3K, Akt rapidly phosphorylates FoxO proteins. The phosphorylated FoxO proteins associate with the 14-3-3 protein, which functions as a scaffold within the cytoplasm, and are sequestered within the cytosol, rendering them unable to bind to the promoters of their target genes in the nucleus to regulate their transcription. In mammals, FoxO subfamily members regulate diverse cell functions such as apoptosis, cell cycle progression, and DNA repair (Accili and Arden, 2004). However, the functional redundancy of FoxO subfamily members makes it difficult to clarify the function of FoxOs in skeletal development (Castrillon et al., 2003; Hosaka et al., 2004).

Akt also regulates the activities of two glycogen synthase kinase 3 (GSK3) proteins, GSK3 α and GSK3 β (Frame and Cohen, 2001). There are three major pools of GSK3 under the basal condition: (1) GSK3 is part of the Wnt signaling complex, which consists of Axin, β -catenin, and other proteins; (2) GSK3 is part of the hedgehog signaling complex, which consists of Cos2, Gli, and other proteins; and (3) there is a free pool of GSK3. Following the binding of Wnt to its receptors, Axin is displaced from GSK3, leading to the stabilization of β -catenin, its accumulation in the nucleus, its binding with members of the Lef/Tcf family of transcription factors, and transcriptional activation of Wnt target genes (Frame and Cohen, 2001). Hedgehog signaling displaces Cos2 from GSK3, inhibiting Gli processing and directing the accumulation of full-length Gli and the transcriptional activation of hedgehog-response genes (Kim and Kimmel, 2006). In the free pool of GSK3, Akt inhibits GSK3 proteins by phosphorylating Ser21 in GSK3 α and Ser9 in GSK3 β . As a result, the residues on glycogen synthase undergo partial dephosphorylation, thereby increasing their activity and hence stimulating glycogen synthesis. GSK3 is a ubiquitously expressed kinase that regulates diverse cellular processes ranging from metabolism to cell fate specification (Cohen and Frame, 2001). The involvement of GSK3 in multiple signaling pathways makes it difficult to clarify the function of the Akt-GSK3 pathway in skeletal development.

Akt activates mTOR through TSC2 and Rheb (Corradetti and Guan, 2006), and activated mTOR plays several important roles in mRNA translation mediated through eukaryotic initiation factor 4E (eIF-4E), which is essential for cap-dependent initiation of translation and promotion of cell growth (Hay and Sonenberg, 2004), and through S6K, which has been implicated in ribosome biogenesis as well as modification of the ribosomal protein, S6 (Hannan et al., 2003). As the IGFs-IGF receptor-PI3K-Akt pathway plays important roles in skeletal development, it is pivotal to clarify the functions of Akt and each of the Akt downstream signaling axes in skeletal development and the molecular linkage to chondrocyte maturation, proliferation, and function.

To pursue these issues, we investigated the roles of Akt signaling pathways during skeletal development, focusing on GSK3, mTOR, and FoxOs, which are predicted to play important roles among the many Akt downstream signaling molecules in the cellular processes of skeletal development. By generating and analyzing chondrocyte-specific constitutively active Akt or dominant negative (dn)-Akt transgenic mice and using organ culture of limb and vertebral skeletons, we show here that chondrocyte maturation and proliferation and cartilage matrix production are regulated by the balance of the three Akt downstream signaling axes of GSK3, mTOR, and FoxOs.

Results

Generation of *myrAkt* transgenic mice

To examine the role of Akt in endochondral ossification, we generated transgenic mice that express constitutively active Akt (*myr*-

istoylated Akt; *myrAkt*) and enhanced green fluorescence protein (EGFP) specifically in chondrocytes using the *Col2a1* promoter (Fig. 1A). As many of the F₀ transgenic mice could not survive after birth, we analyzed the transgenic mice at embryonic stages. We selected 64 F₀ embryos with EGFP expression from a total of 747 embryos (Fig. 1B). To estimate expression levels of the transgene, all embryos were selected by EGFP intensities, and the expression level of the transgene in some EGFP-positive embryos was analyzed by Northern blot analysis with the *Akt* probe (Fig. 1C). The transgenic embryos whose expression level of the transgene was less than half of that of endogenous Akt were classified as tg(L), and the transgenic embryos whose expression level of the transgene was more than half of that of endogenous Akt were classified as tg(H). The other EGFP-positive embryos were classified as tg(L) (total 39 pups) or tg(H) (total 25 pups) by comparing the intensities of EGFP. The body size of tg(L) was enlarged, but the limbs of tg(H) were shortened (Fig. 1B). The EGFP signals in the embryos at embryonic day 18.5 (E18.5) showed that the transgene was expressed in a cartilage-specific manner (Fig. 1D), and the signals were strongly detected in resting and proliferating chondrocytes (Figs. 1E, F). Immunohistochemistry using anti-GFP antibody showed that some of the hypertrophic chondrocytes, which were enlarged, also expressed the transgene strongly (Fig. 1G), although the number of the hypertrophic chondrocytes, which strongly expressed transgene, was limited and variable in individual F₀ transgenic mouse (data not shown).

myrAkt transgenic mice had thickened limb skeletons with reduced mineralization and enlarged craniobasal and vertebral skeletons with enhanced mineralization

To assess the process of endochondral ossification in *myrAkt* transgenic mice, the skeletons at E15.5 and E18.5 were stained with Alcian blue and Alizarin red to detect cartilage and calcified tissue, respectively (Figs. 1H–O). All of the skeletal elements of endochondral bones, including limb bones, ribs, craniobasal bones, and vertebrae, were thickened or enlarged in tg(L) at E15.5 (Figs. 1H–J, data not shown) and E18.5 (Figs. 1K–O). The mineralization of limb skeletons in tg(L) was reduced compared with that in wild-type mice at E15.5 (Figs. 1H, I). In tg(H), the limb skeletons, sternum, and ribs were thick but the length was diminished and the mineralization of limb skeletons was reduced compared with those in wild-type embryos at E18.5 (Figs. 1K–M). However, the mineralization of the sphenoid bone, basioccipital bone, and vertebrae was advanced in *myrAkt* transgenic mice in a manner dependent on transgene expression (Figs. 1N and O). Further, the primordium of the petrous part of the temporal bone was mineralized in tg(L) and tg(H) but not in wild-type embryos (Fig. 1N). These findings indicate that constitutive activation of Akt in chondrocytes thickens or enlarges all of the endochondral bones and enhances mineralization of the craniobasal and vertebral skeletons but inhibits mineralization of limb skeletons, and that high expression of constitutively active Akt inhibits longitudinal growth of limb, sternum, and rib skeletons.

Deceleration of chondrocyte maturation in limb skeletons and acceleration of chondrocyte maturation in craniobasal and vertebral skeletons of myrAkt transgenic mice

As endochondral ossification was retarded in limb skeletons of *myrAkt* transgenic mice (Figs. 1H, I, K, L), we examined chondrocyte maturation in tibiae at E13.5 and E15.5 by *in situ* hybridization (Fig. 2). At E13.5, *Col2a1* mRNA, which is expressed in resting and proliferating chondrocytes, was detected in wild-type, tg(L), and tg(H) tibiae, while *Pthr1* mRNA, which is expressed in prehypertrophic chondrocytes and early hypertrophic chondrocytes, was detected in wild-type tibiae but was barely detectable in tg(L) and tg(H) tibiae (Figs. 2A–C). At E15.5, the length of the proliferating chondrocyte layer was diminished in

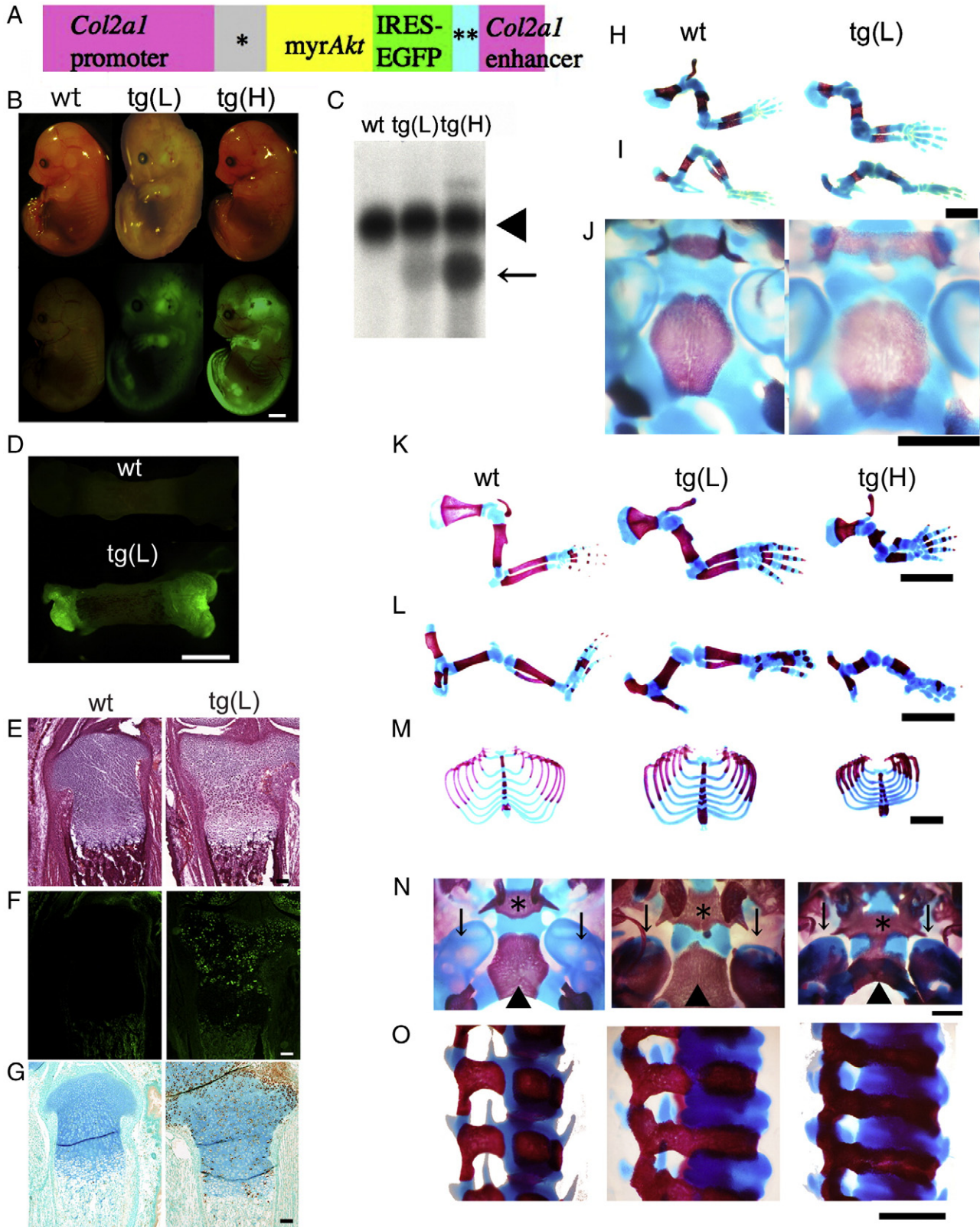


Fig. 1. Generation of *myrAkt* transgenic mice and examination of the skeletal system. (A) Diagram of the DNA construct used to generate *Col2a1*-*myrAkt* transgenic mice. *SV40 splice donor/acceptor sequences, **SV40 polyadenylation sequence. (B) Gross appearance and EGFP fluorescence of wild-type (wt) mouse, tg(L), and tg(H) at E15.5. The pictures of bright field (upper panel) and dark field (lower panel) are shown. (C) Northern blot analysis with the Akt probe. RNA was extracted from the skeletons of wild-type mice (wt), tg(L), and tg(H) at E18.5. The arrowhead shows endogenous Akt mRNA and the arrow shows transgene mRNA. (D–G) EGFP fluorescence in whole femurs (D) and in the frozen sections of femurs (E) and immunohistochemical analysis of EGFP protein using the paraffin-embedded sections of femurs (F) from wild-type mouse and tg(L) at E18.5. Sections in F were stained with HE. A nonspecific fluorescent signal was detected in the region of the primary spongiosa and bone collar (F). The sections in G were counterstained with methyl green. (H–O) Skeletal system at E15.5 (H–J) and E18.5 (K–O). Forelimbs (H, K), hind limbs (I, L), cranial bases (J, N), thoracic cages (M), and vertebrae (O) of wild-type mice, tg(L) and tg(H) are shown. Asterisks show sphenoid bones, arrowheads show basioccipital bones, and arrows show the petrous part of the temporal bones (N). Scale bars: (B, D, J, N, O) 1 mm; (E–G) 200 μ m; (H, I, K, M) 2 mm; (L) 3 mm.

myrAkt transgenic mice compared with wild-type mice in a manner dependent on transgene expression (Figs. 2D, 3A, B, F, G). In situ hybridization of wild-type tibiae at E15.5 showed the following: *Col2a1* mRNA was detected in the epiphyses; *Pthr1* and *Col10a1* mRNAs, the latter of which is expressed in hypertrophic chondrocytes, were detected in the metaphyses; and *Spp1* mRNA, which is expressed in terminal hypertrophic chondrocytes and osteoblasts, was detected in the diaphysis (Figs. 2E–H). In tg(L) and tg(H), however, *Col2a1* mRNA was detected in the epiphyses and metaphyses, *Pthr1* and *Col10a1* mRNAs were detected in the diaphyses, and *Spp1* mRNA was not detected (Figs. 2E–H), indicating that chondrocyte maturation was retarded in *myrAkt* transgenic mice. The mRNA of *Ihh*, which plays important roles in chondrocyte maturation and proliferation, was detected in prehypertrophic chondrocytes and early hypertrophic chondrocytes at similar levels in wild-type mice, tg(L), and tg(H) at E15.5 (Supplementary Fig. 1A, data not shown).

As endochondral ossification was accelerated in craniobasal and vertebral skeletons (Figs. 1J, N, and O), we examined chondrocyte maturation at E15.5 by von Kossa staining and in situ hybridization. In wild-type mice, the basioccipital bone was not mineralized and *Col10a1* expression was detected in the middle part of this bone (Figs. 2I and J). In tg(L), however, the basioccipital bone was enlarged, a large area of the bone was mineralized, and the mineralized area separated the two *Col10a1*-positive layers by a large distance. Hypertrophy accompanying *Col10a1* expression was evident in the vertebrae of tg(L) compared with wild-type mice (Figs. 2K and L). These findings indicate that chondrocyte maturation was accelerated in craniobasal cartilaginous elements and vertebrae of *myrAkt* transgenic mice.

We next examined the expression levels of *Pthlh*, *Ihh*, and *Runx2* by real-time RT-PCR using the RNA from long bones and vertebrae at E15.5. The levels of *Pthlh*, *Ihh* and *Runx2* mRNA expression in the limb and vertebral skeletons did not significantly differ between wild-type mice and tg(L) (Supplementary Fig. 1C).

Enhanced chondrocyte proliferation in vertebrae and in resting but not in proliferating layers of limb skeletons and increased cartilage matrix in myrAkt transgenic mice

As the length of the proliferating layer of tibiae was diminished in *myrAkt* transgenic mice, we examined chondrocyte proliferation in tibiae at E15.5 by BrdU labeling (Figs. 3A–E). The frequency of BrdU-positive cells in the resting layer of tg(L) was increased compared with that in wild-type mice, whereas the frequency in the proliferating layer of tg(L) was reduced (Figs. 3A, B, E). In vertebrae, the frequency of BrdU-positive cells was increased throughout the entire region except the hypertrophic zone in tg(L) compared with wild-type mice (Figs. 3C–E).

To evaluate the effect of Akt activation on cartilage matrix production, we performed staining with safranin O, which stains proteoglycans, and immunohistochemical analysis of type II collagen using sections from tibiae and vertebrae (Figs. 3F–N). Although the intensities of staining with safranin O and immunoreactivity against type II collagen in tibiae or vertebrae were similar between wild-type mice and tg(L), the extracellular matrix area was increased in the resting and proliferating layers of tibiae and in the vertebrae of tg(L) compared with wild-type mice (Figs. 3F–N). Further, limb mesenchymal cells from tg(L) at E12.5 produced more cartilaginous matrix than those from wild-type mice in vitro (Fig. 3O). These findings indicate that extracellular matrix production was enhanced in tg(L). As the levels of *aggrecan* and *Col2a1* mRNA expression seemed to be similar between wild-type and *myrAkt* transgenic mice, it is suggested that cartilage matrix production was enhanced at the post-transcriptional level (Fig. 2E, Supplementary Fig. 1B). Cell size of chondrocytes was also enlarged in the proliferating layer of tibiae and in the region without hypertrophy

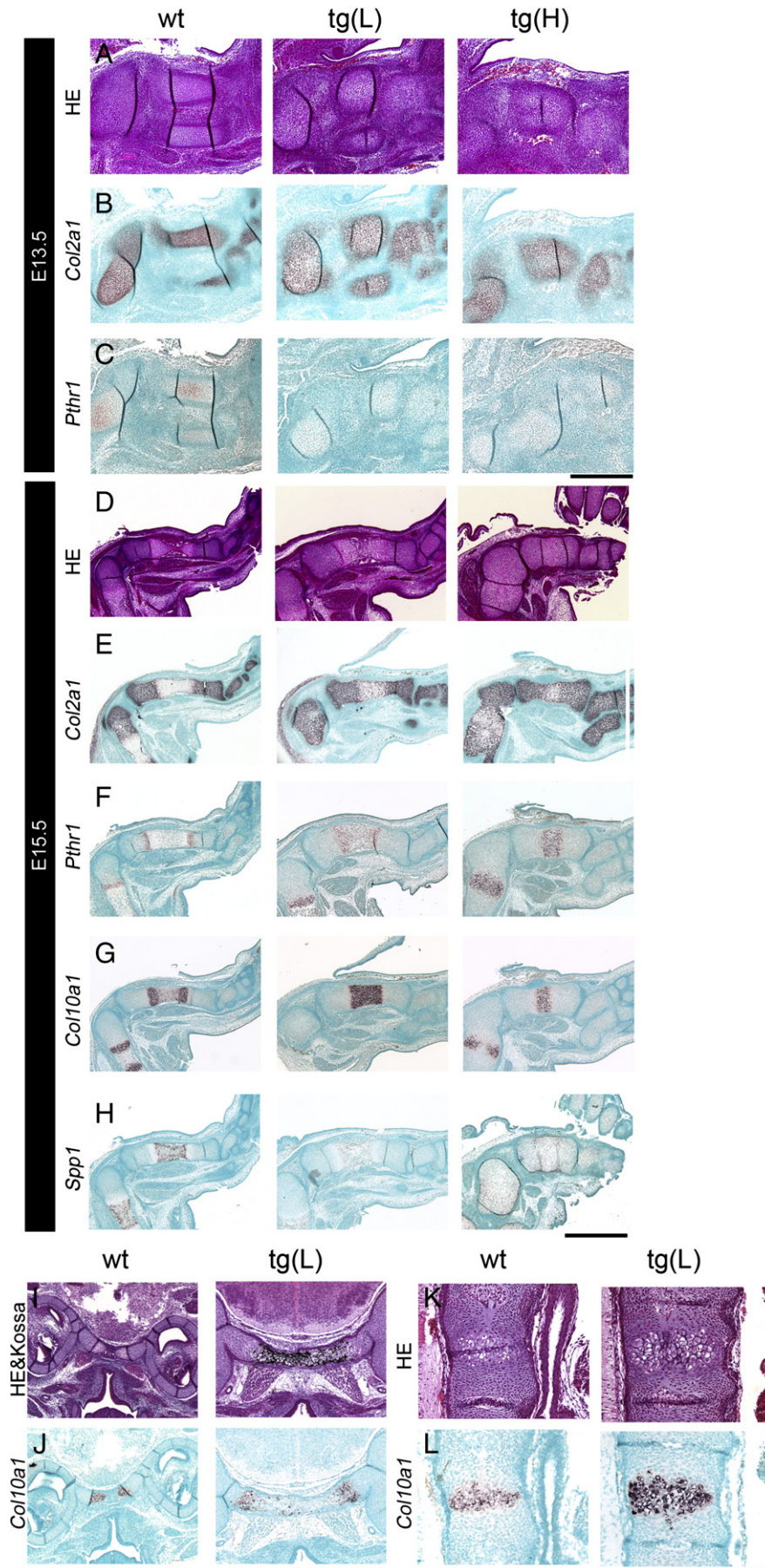
in the vertebrae of tg(L) (Fig. 3P). Further, the size of the hypertrophic chondrocytes in tibiae of tg(L) was approximately 1.5-fold of that in wild-type mice (Fig. 3P). The resting layer in tg(L) was enlarged due to the increased chondrocyte proliferation and matrix production, whereas the proliferating layer was shortened due to the reduced chondrocyte proliferation and the columnar structure was disorganized due to the increased matrix production and increased cell size (Figs. 3A, B, E, H, I, N, P). No vascular invasion was observed in the resting and proliferating layers of growth plates in tg(L) and tg(H) (Figs. 2, 3).

Endochondral ossification was retarded in the whole skeleton of dn-Akt transgenic mice

We also generated transgenic mice expressing dn-Akt, which inhibited PDGF-induced phosphorylation of Akt in ATDC5 cells (Supplementary Fig. 2A), under the control of the *Col2a1* promoter (Supplementary Fig. 2B–D). We obtained 46 F₀ transgenic embryos with an EGFP signal from a total of 521 embryos. However, only 3 F₀ transgenic embryos had high transgene expression, the level of which was similar to that of endogenous Akt, and their data are shown here. The other 43 F₀ transgenic embryos had a low level of transgene expression of less than half of that of endogenous Akt, and their phenotype did not significantly differ from that of wild-type littermates (data not shown), probably due to the high level of endogenous Akt expression (Supplementary Fig. 2D). At E15.5, the skeleton was smaller and thinner and mineralization of the limbs, ribs, and cervical vertebrae was reduced in dn-Akt transgenic mice compared with wild-type mice (Figs. 4A, B). The retardation of endochondral ossification was due to the deceleration of chondrocyte maturation, as shown by the delayed appearance of hypertrophic chondrocytes that express *Col10a1* in the tibia and basioccipital bone (Figs. 4C–J). At E18.5, the vertebral bodies were smaller and less mineralized and chondrocyte hypertrophy accompanied by *Col10a1* expression was delayed in dn-Akt transgenic mice compared with wild-type mice (Figs. 4K–O). Cartilage matrix production and chondrocyte proliferation were reduced in both the resting and proliferating layers of tibiae of dn-Akt transgenic mice compared with wild-type mice (Figs. 4P–S, Supplementary Fig. 2E). Apoptotic cells were rare in the resting and proliferating layers of growth plates in wild-type mice, tg(L), and dn-Akt transgenic mice by TUNEL staining, although TUNEL-positive cells were observed in the corresponding layers of tg(H) (data not shown). These findings indicate that dn-Akt inhibited chondrocyte maturation, chondrocyte proliferation and cartilage matrix production, leading to the small skeleton.

Expression of Akt, Akt downstream signaling molecules, GSK3 β , S6K, and FoxO3a, and their phosphorylated forms in growth plates

We examined the expression of Akt, GSK3 β , S6K, FoxO3a, and their phosphorylated forms in the growth plates of wild-type and *myrAkt* transgenic mice by immunohistochemistry (Fig. 5). Akt and phosphorylated Akt were detected in all regions of the growth plates of wild-type and *myrAkt* transgenic mice with higher levels in *myrAkt* transgenic mice (Figs. 5A–D). GSK3 β was weakly expressed in the resting chondrocytes, upregulated in the proliferating layer, and strongly expressed in the hypertrophic chondrocytes in both wild-type and *myrAkt* transgenic mice (Figs. 5E, F). Phosphorylated GSK3 β was detected in a similar pattern in wild-type mice, but it was strongly detected in all regions of the growth plates of *myrAkt* transgenic mice (Figs. 5G, H). S6K, FoxO3a, and their phosphorylated forms were detected in all regions of the growth plates of wild-type and *myrAkt* transgenic mice, although higher levels of the phosphorylated forms were detected in *myrAkt* transgenic mice than wild-type mice (Figs. 5I–P). These findings indicate that the Akt downstream signaling



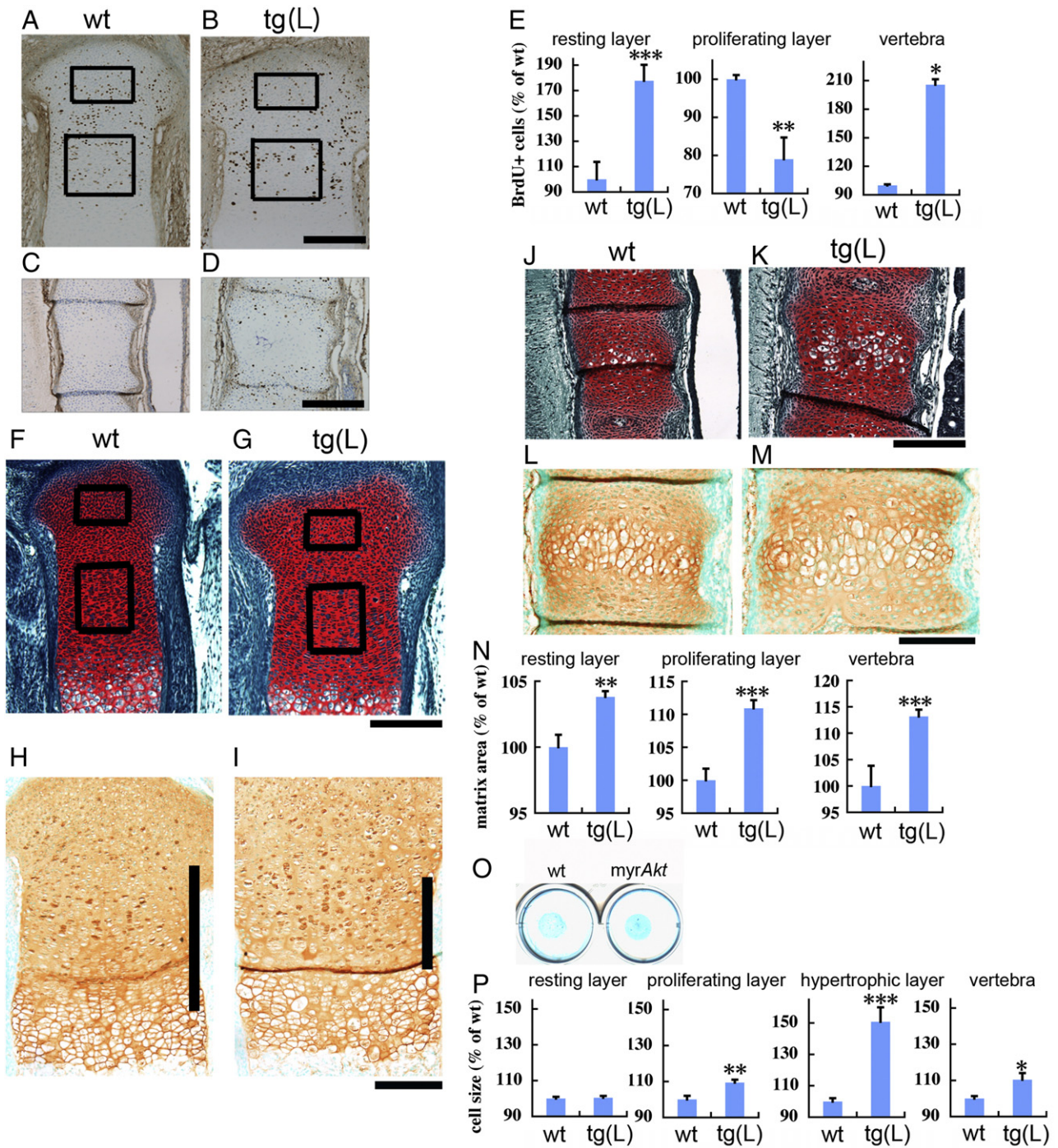


Fig. 3. Chondrocyte proliferation, cartilage matrix production, and cell growth in *myrAkt* transgenic mice. (A–E) BrdU labeling. Using sections of tibiae (A, B) and vertebrae (C, D) from wild-type mice (A, C) and *tg(L)* (B, D) at E15.5, BrdU-positive cells were counted in the resting layers (upper boxes in A and B) and proliferating layers (lower boxes in A and B) of tibiae and in vertebrae (E). BrdU-positive cells in vertebrae were counted in an arbitrary area without hypertrophic chondrocytes. (F–N) Increased extracellular matrix area in *tg(L)*. Sections of tibiae (F–I) and vertebrae (J–M) from wild-type mice (F, H, J, L) and *tg(L)* (G, I, K, M) at E15.5 (F, G, J, K) and E18.5 (H, I, L, M) were stained with Safranin O (F, G, J, K) or reacted with anti-type II collagen antibody (H, I, L, M), and the extracellular matrix area was calculated in the resting layers (upper boxes in F and G) and proliferating layers (lower boxes in F and G) of tibiae and in vertebrae (N). Bars in H and I show the proliferating layer. Note that the proliferating layer in *tg(L)* (I) is short and disorganized as compared with wild-type mice (H). (O) Micromass culture of limb mesenchymal cells. Mesenchymal cells from limbs of wild-type mice and *tg(L)* at E12.5 were cultured for 7 days and stained with Alcian blue. A representative picture from three independent experiments is shown. (P) Cell sizes of chondrocytes were calculated in the resting, proliferating, and hypertrophic layers of tibiae and in vertebrae. Relative values are shown as a percentage of the mean value in wild-type mice in E, N, and P. Data are presented as mean \pm S.E. of 5 mice. * $P < 0.05$, ** $P < 0.01$, *** $P < 0.005$ vs. wild-type mice. Scale bars: (A, B, F, G) 70 μ m; (C, D, J, K) 50 μ m; (H, I, L, M) 200 μ m.

Fig. 2. Endochondral ossification in limbs, cranial base, and vertebrae of *myrAkt* transgenic mice. Serial sections of limbs (A–H), cranial bases (I, J), and vertebrae (K, L) of wild-type (*wt*) mice, *tg(L)* and *tg(H)* were examined by HE staining (A, D, K), HE and von Kossa staining (I), and in situ hybridization using *Col2a1* (B, E), *Pthr1* (C, F), *Col10a1* (G, J, L), and *Spp1* (H) probes at E13.5 (A–C) and E15.5 (D–L). Note that the chondrocranium was markedly enlarged in *tg(L)* (I, J). Scale bars: (A–J) 500 μ m; (K, L) 200 μ m.

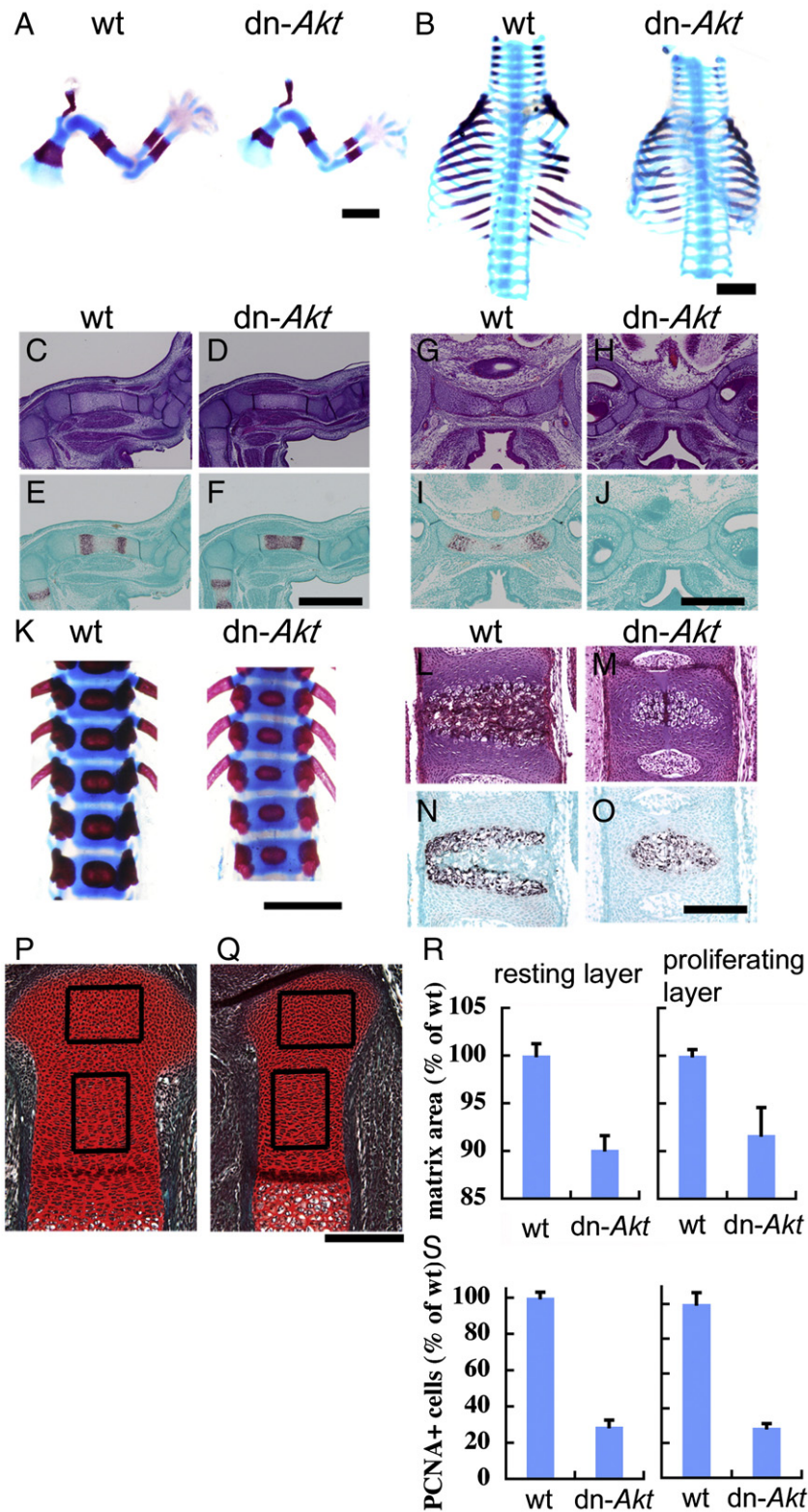


Fig. 4. Endochondral ossification, chondrocyte maturation and proliferation, and cartilage matrix production in *dn-Akt* transgenic mice. (A and B) Skeletal system at E15.5. Forelimbs (A) and thoracic cages and vertebrae (B) of wild-type and *dn-Akt* transgenic mice are shown. (C–J) Histological analysis of hind limbs (C–F) and cranial bases (G–J) at E15.5. Serial sections of hind limbs (C–F) and cranial bases (G–J) of wild-type mice (C, E, G, I) and *dn-Akt* transgenic mice (D, F, H, J) were examined by HE staining (C, D, G, H) and in situ hybridization using *Col10a1* probe (E, F, I, J). (K–O) Endochondral ossification of vertebrae at E18.5. The skeletal system of vertebrae (K) and results of the histological examination by HE staining (L, M) and in situ hybridization using *Col10a1* probe (N, O) using serial sections of vertebrae of wild-type mice (L, N) and *dn-Akt* transgenic mice (M, O) are shown. In the comparison of wild-type and *dn-Akt* transgenic F_0 embryos, we always compared the littermates, because the developmental stages of wild-type F_0 embryos were similar among littermates but frequently not among unrelated wild-type F_0 embryos as seen in Figs. 21–L and Figs. 4G, I, L, N. (P–R) Reduced cartilage matrix production in *dn-Akt* transgenic mice. Sections of tibiae from wild-type mice (P) and *dn-Akt* transgenic mice (Q) at E15.5 were stained with Safranin O, and extracellular matrix area was calculated in the resting layers (upper boxes in P and Q) and proliferating layers (lower boxes in P and Q) of tibiae (R). (S) Chondrocyte proliferation. PCNA-positive cells were counted in the resting layers and proliferating layers of tibiae. Relative values are shown as a percentage of the respective control. Data represent the mean \pm S.E. of two wild-type mice and two *dn-Akt* transgenic mice. Scale Bar: (A, B, K) 1 mm; (C–F) 500 μ m; (G–J) 500 μ m; (L–Q) 50 μ m.

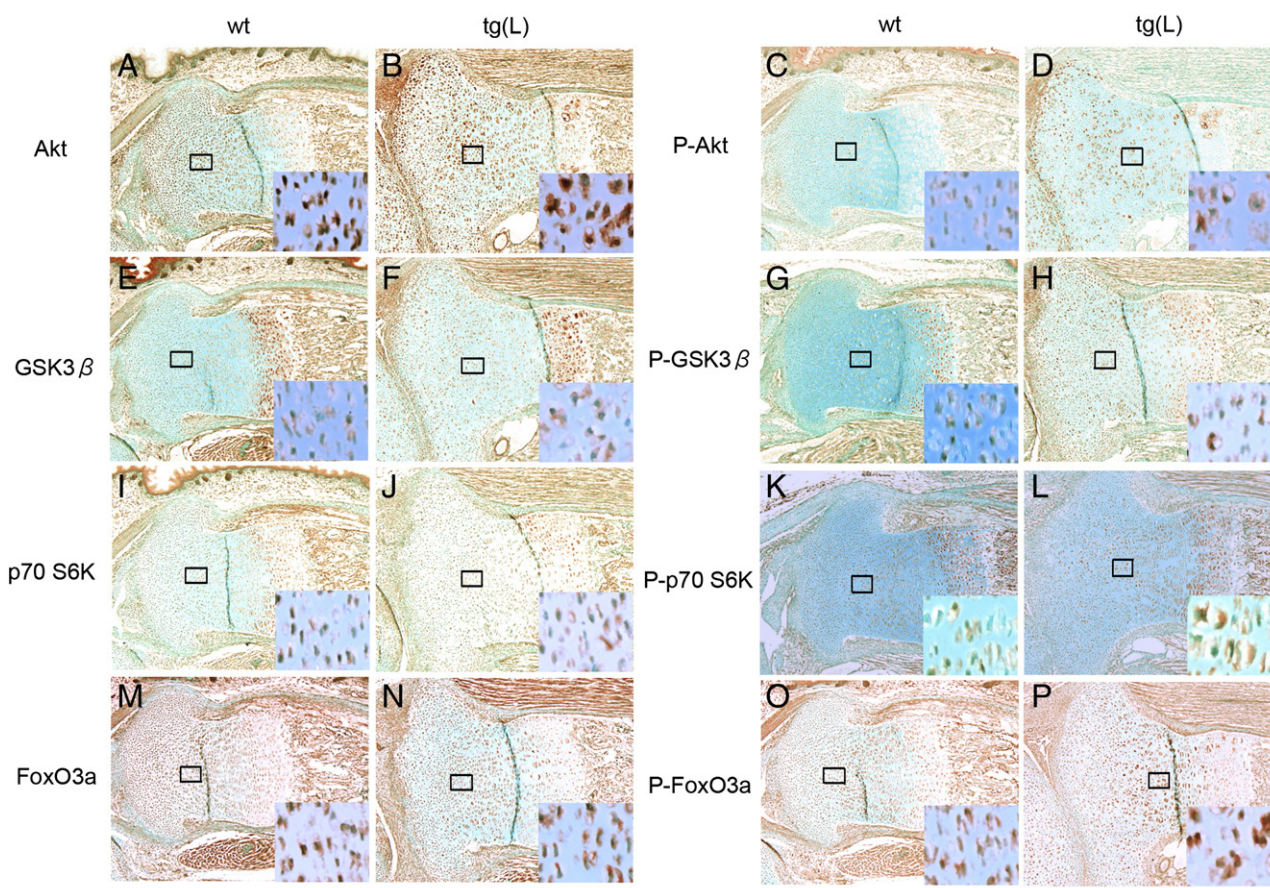


Fig. 5. Detection of Akt, GSK3 β , p70 S6K, and FoxO3a proteins and their phosphorylated forms in growth plates. Immunohistochemical analyses were performed on sections of femurs of wild-type mice (A, C, E, G, I, K, M, and O) and tg(L) (B, D, F, H, J, L, N, P) at E18.5 using anti-Akt (A, B), anti-phosphorylated Akt (C, D), anti-GSK3 β (E, F), anti-phosphorylated GSK3 β (G, H), anti-p70 S6K (I, J), anti-phosphorylated p70 S6K (K, L), anti-FoxO3a (M, N), and anti-phosphorylated FoxO3a (O, P) antibodies. The boxed regions are magnified in the respective insets. P; phosphorylated. Scale bar: 200 μ m.

pathways, Akt-GSK3, Akt-mTOR, and Akt-FoxO, are stimulated by the activation of Akt in growth plates.

Mechanisms of the regulation of limb skeletal development by Akt downstream signaling molecules

To elucidate the molecular mechanism of Akt functions in the cellular processes of skeletal development, we further examined the functions of the Akt downstream signaling pathways. To analyze their functions in chondrocyte maturation, chondrocyte proliferation, cartilage matrix production, and cell growth in limb skeletons, we examined the effect of treatment with lithium chloride, a GSK inhibitor, or rapamycin, an mTOR-specific inhibitor, and overexpression of *FoxO3a*-TM (constitutively active form, in which the three Akt phosphorylation sites were mutated) or dn-*FoxO3a* in organ cultures of limb skeletons from wild-type mice at E15.5 (Fig. 6, Supplementary Fig. 3A). First, we confirmed the effectiveness of lithium chloride and rapamycin by immunohistochemistry using anti- β -catenin antibody and anti-phosphorylated p70 S6K antibody, respectively. Treatment with lithium chloride accumulated β -catenin to the nuclei and treatment with rapamycin reduced the phosphorylation of p70 S6K (Figs. 6A, B). Treatment with either lithium chloride or rapamycin reduced mineralization and reduced the length of the hypertrophic layers compared with those on the side treated with vehicle. Introduction of *FoxO3a*-TM or dn-*FoxO3a* increased or decreased mineralization and increased or decreased the length of the hypertrophic layers, respectively, compared with those upon introduction of EGFP (Figs. 6C, D). These findings indicate

that GSK3, mTOR, and FoxOs all positively regulate chondrocyte maturation.

Treatment with either lithium chloride or rapamycin reduced the extracellular matrix area in the resting and proliferating layers of femurs compared with those in vehicle-treated femurs. Introduction of *FoxO3a*-TM or dn-*FoxO3a* increased or decreased the extracellular matrix area, respectively, in resting and proliferating layers of femurs compared with those in EGFP-infected femurs (Fig. 6E). In accordance with the data from the organ cultures, cartilaginous matrix production was inhibited by treatment with either lithium chloride or rapamycin and enhanced by the introduction of *FoxO3a*-TM in the micromass culture of primary chondrocytes (Supplementary Fig. 3C). Further, the cell size of chondrocytes in the resting and proliferating layers of femurs was reduced by treatment with rapamycin but not by treatment with lithium chloride, *FoxO3a*-TM, or dn-*FoxO3a* compared with that in the respective control (Fig. 6F). These findings indicate that GSK3, mTOR, and FoxOs all positively regulate cartilage matrix production, and that mTOR positively regulates cell growth.

To investigate chondrocyte proliferation, tibiae in organ culture were labeled with BrdU. Treatment with either lithium chloride or rapamycin severely reduced the number of BrdU-positive cells in resting and proliferating layers compared with that in vehicle-treated tibiae. Adenoviral introduction of *FoxO3a*-TM or dn-*FoxO3a* reduced or increased the percentage of BrdU-positive cells, respectively, in the resting and proliferating layers of tibiae compared with those in tibiae infected with EGFP adenovirus (Fig. 6G, Supplementary Fig. 3D). These findings indicate that GSK3 and mTOR positively regulate chondrocyte proliferation while FoxOs negatively regulate it.

Effect of Akt-GSK3 signaling on chondrocyte maturation, chondrocyte proliferation and cartilage matrix production in limb skeletons

Treatment with lithium chloride enhanced the expression of TOP-flash and Gli-reporter constructs (Figs. 7A, B), indicating that lithium chloride enhances canonical Wnt signaling and hedgehog signaling by inhibiting GSK3. To specify the effect of Akt-GSK3 signaling, therefore, we first examined the effects of canonical Wnt signaling and hedgehog signaling on chondrocyte maturation, chondrocyte proliferation, extracellular matrix production, and cell growth by organ culture of limb skeletons (Figs. 7C–G). Treatment with Wnt3a or adenoviral introduction of dn-*Tcf* inhibited or enhanced, respectively, endochondral ossification and chondrocyte maturation (Figs. 7C, D). Adenoviral introduction of *Gli* or dn-*Gli* inhibited or enhanced, respectively, endochondral ossification and chondrocyte maturation (Figs. 7C, D). Therefore, both canonical Wnt signaling and hedgehog signaling negatively regulated endochondral ossification by inhibiting chondrocyte maturation. The extracellular matrix area was increased by either dn-*Tcf* or dn-*Gli*, indicating that cartilage matrix production is negatively regulated by canonical Wnt signaling and hedgehog signaling (Fig. 7E). Cell size of chondrocytes was not affected by either signaling pathway (Fig. 7F). Chondrocyte proliferation was enhanced by dn-*Tcf* but inhibited by dn-*Gli*, indicating that canonical Wnt signaling inhibits but hedgehog signaling enhances chondrocyte proliferation (Fig. 7G). Next, we examined the effect of lithium chloride in the presence of both dn-*Tcf* and dn-*Gli*, which efficiently inhibited expression of the respective reporter gene even in the presence of lithium chloride (Figs. 7A, B). Treatment with lithium chloride inhibited chondrocyte maturation, chondrocyte proliferation and extracellular matrix production in the condition in which both canonical Wnt signaling and hedgehog signaling were blocked (Figs. 7C–E, G). These findings indicate that the free pool of GSK3, which is phosphorylated by Akt, MAPKAP-K1, and S6K (Frame and Cohen, 2001), has positive effects on chondrocyte maturation, chondrocyte proliferation and cartilage matrix production in limb skeletons.

Mechanisms of the regulation of vertebral development by Akt downstream signaling molecules

To investigate the downstream signaling pathways of Akt in vertebral development, we performed organ culture using wild-type vertebrae at E16.5. Treatment with the GSK3 inhibitors, SB216763 or lithium chloride, did not affect the size of the vertebral bodies, mineralization, chondrocyte hypertrophy, extracellular matrix area, cell size of chondrocytes, nor chondrocyte proliferation, and treatment with increased concentrations of lithium chloride also failed to affect the size of the vertebral bodies and mineralization (Figs. 8A–E, Supplementary Fig. 4A, data not shown). In contrast, treatment with rapamycin reduced the size of the vertebral bodies, mineralization, number of hypertrophic chondrocytes, extracellular matrix area, cell size of chondrocytes, and chondrocyte proliferation compared with the respective parameter in vehicle-treated vertebrae (Figs. 8A–E, Supplementary Fig. 3E). Adenoviral introduction of *FoxO3a*-TM or dn-*FoxO3a* increased or decreased, respectively,

the size of the vertebral bodies, the area of mineralization, number of hypertrophic chondrocytes, and extracellular matrix area, and decreased or increased chondrocyte proliferation, respectively, compared with the adenoviral introduction of EGFP (Figs. 8A–E, Supplementary Fig. 3E).

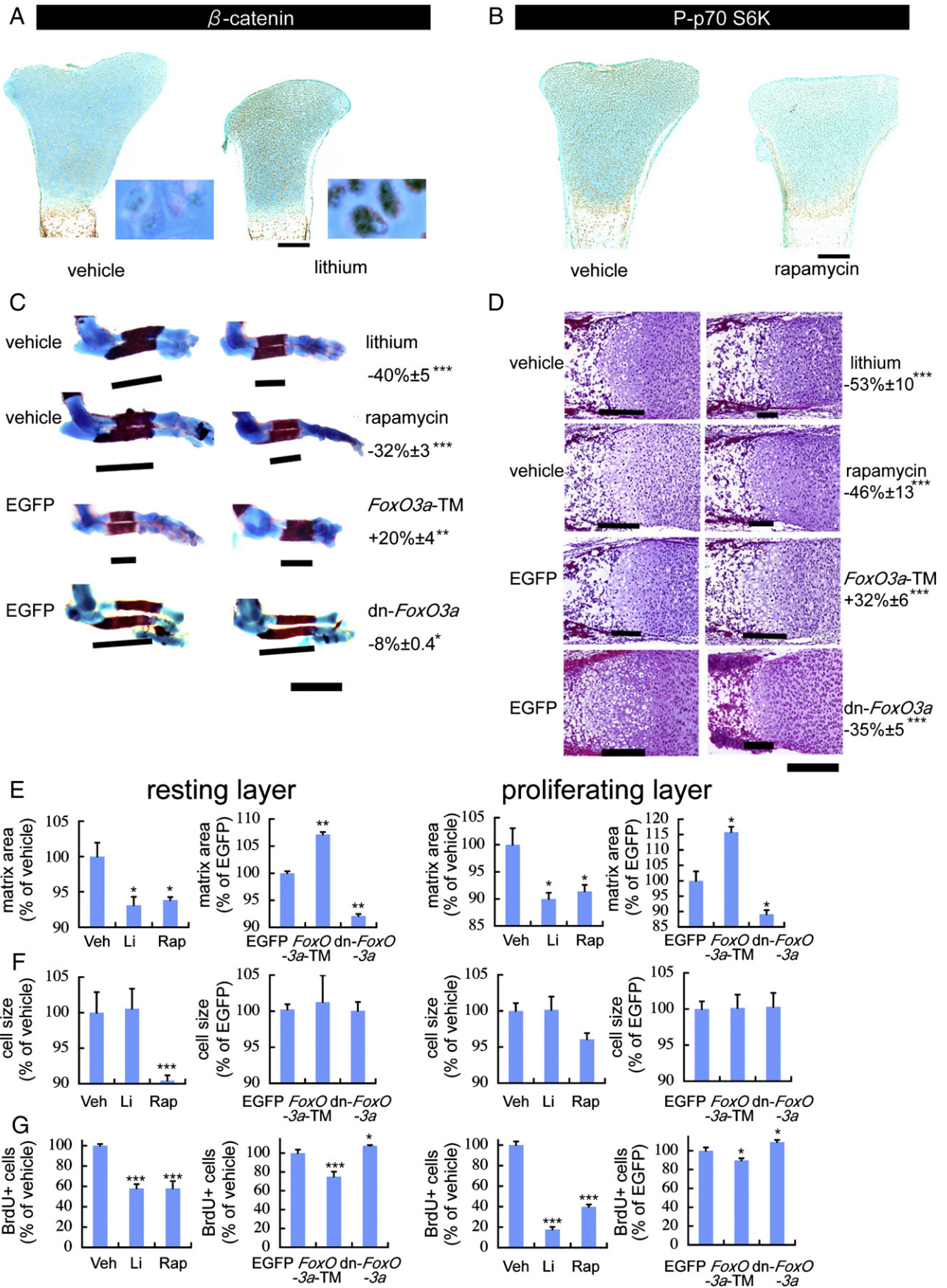
Adenoviral introduction of either dn-*Tcf* or dn-*Gli* increased the area of mineralization, the number of hypertrophic chondrocytes, and extracellular matrix area compared with the adenoviral introduction of EGFP, indicating that canonical Wnt signaling and hedgehog signaling inhibit chondrocyte maturation and cartilage matrix production in vertebrae (Figs. 8F–H). Adenoviral introduction of dn-*Tcf* or dn-*Gli* enhanced or inhibited chondrocyte proliferation, respectively, indicating that canonical Wnt signaling inhibits and hedgehog signaling enhances chondrocyte proliferation in vertebrae (Fig. 8J). However, treatment with lithium chloride showed no additional effects on chondrocyte maturation, extracellular matrix area, and chondrocyte proliferation in the presence of dn-*Tcf* or dn-*Gli* or in the presence of both dn-*Tcf* and dn-*Gli* in vertebrae (Figs. 8F–H, J, Supplementary Fig. 4B–D, F). Cell size of chondrocytes was not affected by the presence of both dn-*Tcf* and dn-*Gli*, and treatment with lithium chloride had no effect on cell size in the presence of dn-*Tcf* or dn-*Gli* or in the presence of both dn-*Tcf* and dn-*Gli* (Fig. 8I, Supplementary Fig. 4E).

The effects and expression of GSK3 in vertebral skeletons

To investigate the reason why the Akt-GSK3 pathway had no significant effects on the cellular processes in vertebrae, we examined the effects of the constitutively active form of GSK3 ($GSK3\beta^{S9A}$) (Supplementary Fig. 5). Adenoviral introduction of $GSK3\beta^{S9A}$ inhibited the expression of TOP-flash and Gli-reporter constructs which was enhanced by Wnt3a and Shh, respectively (Supplementary Fig. 5A, B). $GSK3\beta^{S9A}$ enhanced endochondral ossification and chondrocyte maturation and increased the extracellular matrix area, and reversed Wnt3a- or Shh-induced inhibition of these cellular processes (Supplementary Fig. 5C–E). $GSK3\beta^{S9A}$ inhibited chondrocyte proliferation and reduced Wnt3a- or Shh-induced chondrocyte proliferation, while $GSK3\beta^{S9A}$ had no significant effect on the cell size of chondrocytes (Supplementary Fig. 5F, G). Further, we examined the effect of lithium chloride in the vertebrae, which was infected with adenovirus expressing $GSK3\beta^{S9A}$. The treatment with lithium chloride abolished the effects of $GSK3\beta^{S9A}$ (Figs. 9A, B). These findings indicate that GSK3 has significant effects not only in limb skeletons but also in vertebrae, and that lithium chloride is effective in vertebrae if GSK3 is introduced.

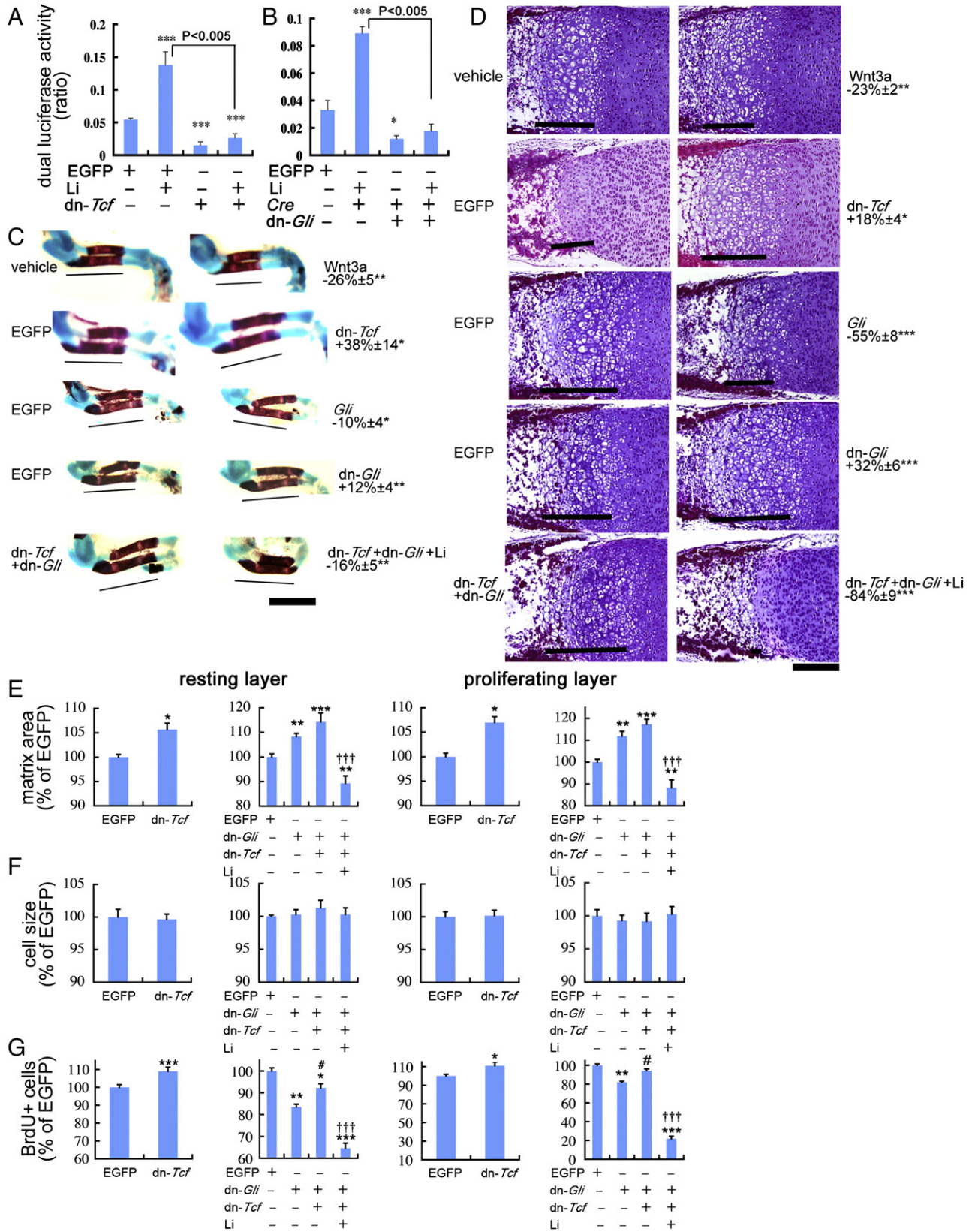
To clarify the reason for the differential effectiveness of lithium chloride in different skeletal parts, we compared GSK3 β expression in limb skeletons and vertebrae on the same section by immunohistochemistry (Figs. 9C–E). In the tibia, GSK3 β expression was increased at the proliferating layer, although the expression level was lower than that in the hypertrophic layer, whereas increased GSK3 β expression was not observed in vertebrae, which lack the proliferating layer. However, GSK3 β expression was also increased in hypertrophic chondrocytes in vertebrae (Fig. 9F). As hypertrophic chondrocytes strongly expressed GSK3 β in both limb skeletons and vertebrae, we extracted protein from Th1-L7 vertebrae, in which

Fig. 6. Functional analysis of Akt downstream signaling pathways in the development of limb skeletons by organ culture. (A, B) Effectiveness of lithium chloride and rapamycin in organ culture. Right tibiae (right panels) of wild-type mice at E15.5 were cultured with 20 mM lithium chloride (lithium) (A) or 10 nM rapamycin (B) for 2 days, while the respective left tibiae (left panels) were cultured with vehicle as controls. The sections were reacted with anti- β -catenin antibody (A) or anti-phosphorylated p70 S6K antibody (B). Regions in the resting layers are magnified in A to visualize the accumulation of β -catenin in the nuclei after the treatment with lithium chloride. (C–F) Skeletal and histological analyses of limb skeletons after organ culture. Right limb skeletons (C and D, right panels) of wild-type mice at E15.5 were cultured with 20 mM lithium chloride (lithium), 10 nM rapamycin, *FoxO3a*-TM adenovirus, or dn-*FoxO3a* adenovirus for 4 days, while the respective left limb skeletons (C and D, left panels) were cultured with vehicle or EGFP adenovirus as controls. The forelimb skeletons were stained with Alcian blue and Alizarin red and the lengths of the calcified regions in ulnae were determined (C, bars). Sections of the hind limb skeletons were stained with HE and the lengths of the hypertrophic layers of femurs were determined (D, bars). Other sections were stained with safranin O, and extracellular matrix area (E) and cell size of chondrocytes (F) in femurs were determined. (G) BrdU incorporation assay. Relative values are shown as a percentage of the respective control. Data are presented as mean \pm S.E. of 5 mice. * $P < 0.05$, ** $P < 0.01$, *** $P < 0.005$ vs the respective control. Scale bars: (A, B) 200 μ m; (C) 2 mm; (D) 50 μ m.



chondrocyte maturation had already occurred (Fig. 9F), and compared it with the protein from limb skeletons by Western blot analysis (Fig. 9G). The protein levels of GSK3 β , phosphorylated GSK3 β , and GSK3 α were less than those in limb skeletons. In contrast, the protein levels of mTOR, phosphorylated mTOR, p70 S6K, phosphorylated p70 S6K,

FoxO3a, and phosphorylated FoxO3a were similar between limb skeletons and vertebrae. Although the levels of hypertrophy in limb skeletons and vertebrae affect the results of Western blot analysis, the results combined with the data from immunohistochemistry indicate that the unresponsiveness of vertebrae to lithium chloride is, at least



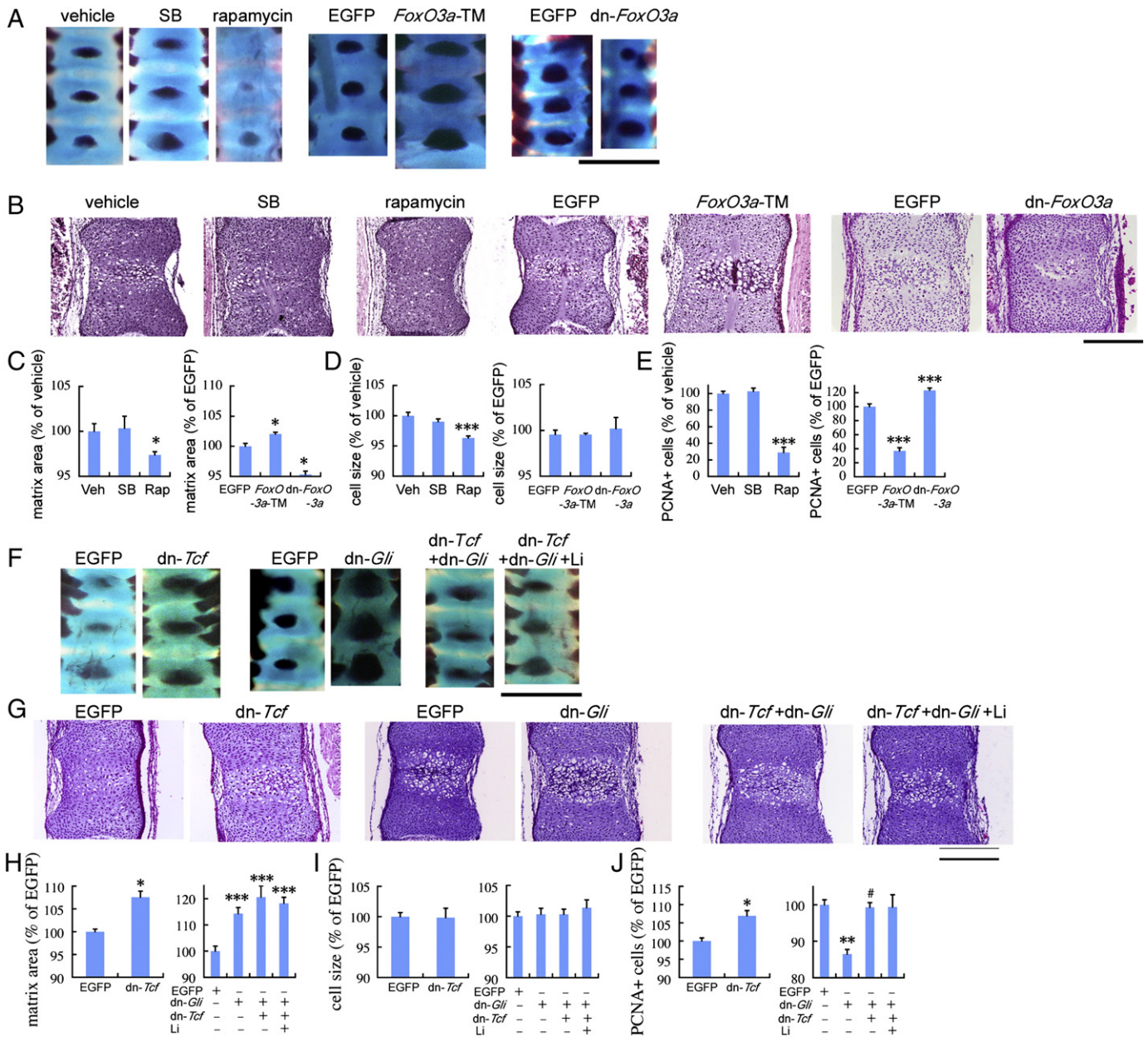


Fig. 8. Functional analysis of Akt downstream signaling pathways in vertebral development by organ culture. (A–E) Vertebral development through Akt downstream signaling pathways. Vertebrae of wild-type mice at E16.5 were cultured with vehicle (Veh), 20 μ M SB216763 (SB), 10 nM rapamycin (Rap), EGFP adenovirus, *FoxO3a*-TM adenovirus, or *dn-FoxO3a* adenovirus. The vertebrae rostral to the second lumbar vertebra (L2), which had been cultured for 4 days, were stained with Alcian blue and Alizarin red (11–13th thoracic vertebrae are shown in A), and sections of the vertebrae caudal to L2, which had been cultured for 2 days, were stained with HE (L6 is shown in B). Serial sections were stained with safranin O, and the extracellular matrix area (C) and cell size of chondrocytes (D) in L6 were determined. (E) PCNA-positive cells in L6. Relative values are shown as the percentage of the respective control. Data are presented as mean \pm S.E. of 5 mice. * P <0.05, *** P <0.005 vs vehicle or EGFP control. (F–J) Vertebral development through canonical Wnt, hedgehog, and Akt signaling pathways. Vertebrae of wild-type mice at E16.5 were cultured with EGFP adenovirus, *dn-Tcf* adenovirus, *dn-Gli* adenovirus, or *dn-Tcf* adenovirus plus *dn-Gli* adenovirus with or without 20 mM lithium chloride (Li). In the infection of *dn-Gli* adenovirus, *Cre* adenovirus was also infected simultaneously to induce *dn-Gli* expression. Skeletal preparations of 11–13th thoracic vertebrae (F) and L6 sections stained with HE (G) are shown. Serial sections of L6 were used for the analyses of extracellular matrix area (H), cell size of chondrocytes (I), and PCNA staining (J). Relative values are shown as a percentage of that in EGFP-adenovirus-infected vertebrae. Data are presented as mean \pm S.E. of 3–5 mice. * P <0.05, ** P <0.01, *** P <0.005 vs EGFP control, # P <0.05 vs *dn-Gli* adenovirus. Scale bars: (A, F) 1 mm; (B, G) 50 μ m.

Fig. 7. Functional analysis of GSK3 in canonical Wnt, hedgehog, and Akt signaling pathways in the development of limb skeletons. (A, B) Reporter assays using TOP-flash (A) and 8 \times Gli-luc reporter constructs (B). The reporter vectors were transfected into chondrogenic ATDC5 cells, and EGFP, *dn-Tcf*, or *dn-Gli* adenovirus was infected into the ATDC5 cells after 24 h. Lithium chloride (Li) at the concentration of 20 mM was added 12 h after the infection, and luciferase activity was determined 48 h later. To induce *dn-Gli* expression, *Cre* adenovirus (*Cre*) was infected 24 h before *dn-Gli* infection. Data are presented as means \pm S.E. of 4 wells. * P <0.05, *** P <0.005 vs EGFP control. (C–F) Skeletal and histological analyses of limb skeletons after organ culture. Right limb skeletons (C and D, right panels) of wild-type mice at E15.5 were cultured with 100 ng/ml of Wnt3a, *dn-Tcf* adenovirus, *Gli* adenovirus, *dn-Gli* adenovirus, or *dn-Tcf* adenovirus plus *dn-Gli* adenovirus with 20 mM lithium chloride for 4 days, while the respective left limb skeletons (C and D, left panels) were cultured with vehicle, EGFP adenovirus or *dn-Tcf* adenovirus plus *dn-Gli* adenovirus as controls. In the infection of *dn-Gli* adenovirus, *Cre* adenovirus was also infected simultaneously to induce *dn-Gli* expression. The lengths of the calcified regions in ulnae were determined (C, bars), and the lengths of the hypertrophic layers in femurs were determined (D, bars). Other sections were stained with safranin O, and the extracellular matrix area (E) and cell size of chondrocytes (F) in femurs were determined. (G) BrdU incorporation assay. Relative values are shown as a percentage of the respective control in C and D, and as a percentage of the EGFP-adenovirus-infected limb skeletons in E–G. Data are presented as mean \pm S.E. of 3–5 mice. * P <0.05, ** P <0.01, *** P <0.005 vs EGFP control, ††† P <0.005 vs *dn-Gli* adenovirus plus *dn-Tcf* adenovirus, # P <0.05 vs *dn-Gli* adenovirus. Scale bars: (C) 2 mm; (D) 50 μ m.

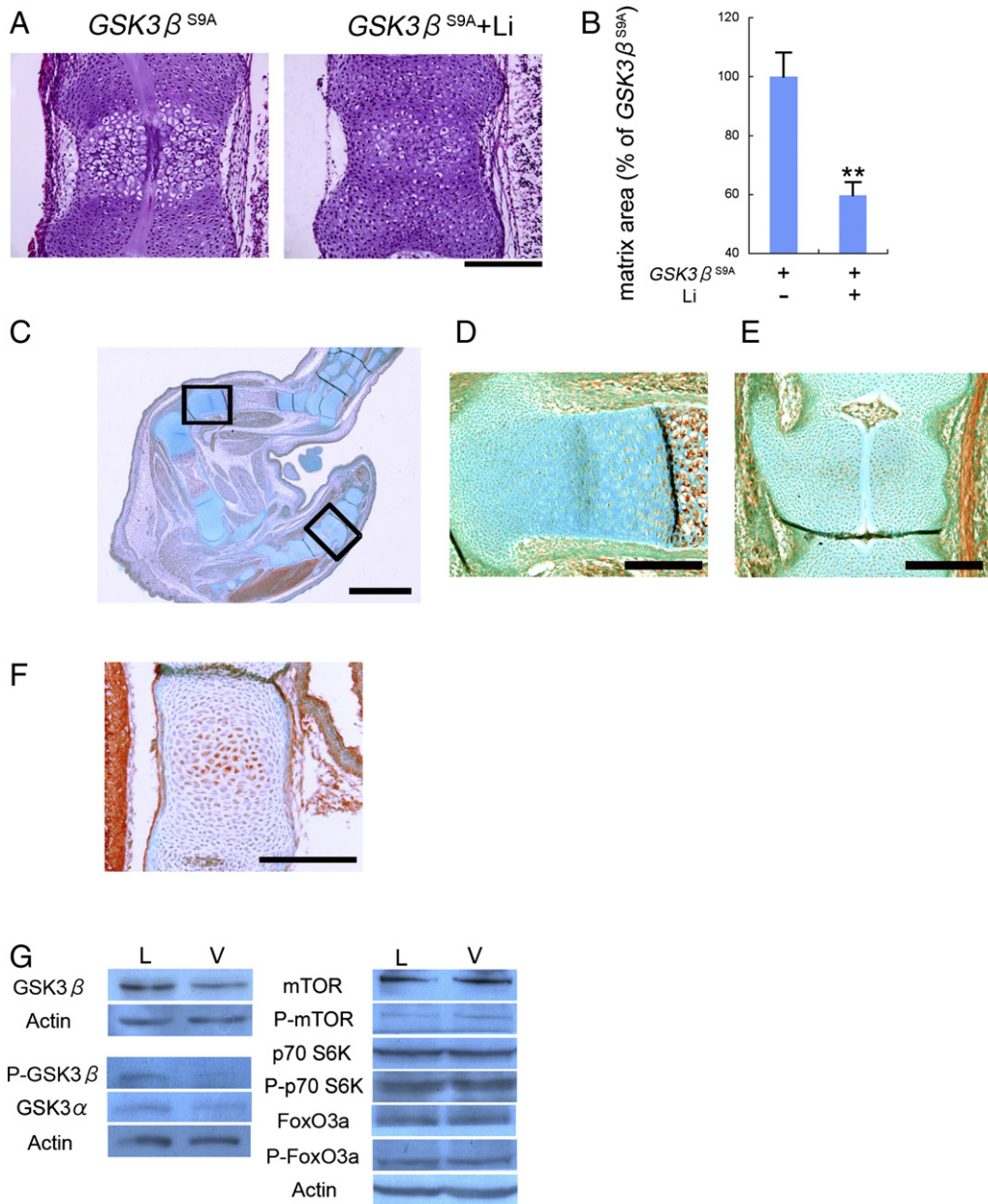


Fig. 9. Expression of GSK3 protein in limb and vertebral skeletons. (A, B) Organ culture of vertebrae. Vertebrae of wild-type mice at E16.5 were cultured with *GSK3β^{S9A}* adenovirus or *GSK3β^{S9A}* adenovirus plus 20 mM lithium chloride (Li) for 2 days, and sections were stained with HE (A). Serial sections were stained with safranin O, and the extracellular matrix area was determined (B). ** $P < 0.01$ vs *GSK3β^{S9A}* adenovirus. (C–F) Immunohistochemical analysis using anti-GSK3β antibody. Sections from wild-type mice at E15.5 were reacted with anti-GSK3β antibody (C, F). The boxed regions in C are magnified in D and E. F shows 10th thoracic vertebra in another section. (G) Western blot analysis. Tissue lysates from limb (L) and vertebral (V) skeletons of wild-type mice at E15.5 were resolved by electrophoresis, blotted, and reacted with anti-GSK3β, anti-phosphorylated GSK3β, anti-GSK3α, anti-mTOR, anti-phosphorylated mTOR, anti-p70 S6K, anti-phosphorylated p70 S6K, anti-FoxO3a, or anti-phosphorylated FoxO3a antibody. Immunoblot with anti-actin antibody was used as an internal control. P; phosphorylated. Scale bars: (A, D–F) 200 μm; (C) 1 mm.

in part, due to a lack of the proliferating layer, in which GSK3β protein expression was upregulated in limb skeletons.

Discussion

Although *Akt1/Akt2*-deficient mice showed dwarfism and the retarded mineralization of the cartilaginous skeletons, the cellular processes of chondrocyte maturation, chondrocyte proliferation, cartilage matrix production, and cell growth were not examined in the mice (Peng et al., 2003). Thus, we first investigated the functions of Akt in skeletal development by analyzing the four cellular processes, using chondrocyte-specific *myrAkt* or *dn-Akt* transgenic mice. Akt positively regulated chondrocyte maturation, chondrocyte prolifera-

tion, cartilage matrix production, and cell growth in the development of limb skeletons and vertebrae, although chondrocyte maturation and chondrocyte proliferation in the proliferating layer were inhibited in limb skeletons of embryos that expressed *myrAkt* (Fig. 10). The Akt downstream signaling molecules, GSK3β, S6K, and FoxO3a, were expressed in the growth plates of wild-type mice, and the levels of their phosphorylation were increased in the growth plates of *myrAkt* transgenic mice compared with wild-type mice, indicating that Akt regulates the phosphorylation of GSK3, mTOR, and FoxO3a in the growth plates. We next examined the functions of the three Akt downstream signaling pathways in the cellular processes of skeletal development by organ culture. As Akt positively regulates mTOR and negatively regulates FoxOs, our findings indicated that the Akt-mTOR

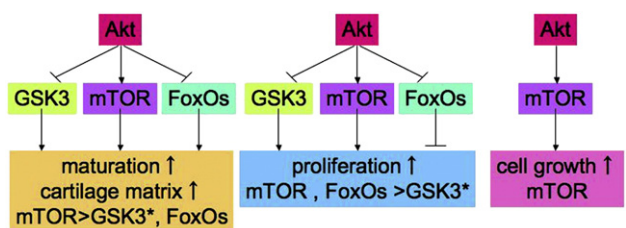


Fig. 10. Schematic representation of the function and predominance of Akt downstream signaling pathways. The function and predominance of Akt downstream signaling pathways, Akt-GSK3, Akt-mTOR, and Akt-FoxOs, in the cellular processes of skeletal development, including chondrocyte maturation, chondrocyte proliferation, cartilage matrix production, and cell growth are shown. Asterisks indicate that the Akt-GSK3 pathway has significant effects on chondrocyte maturation, chondrocyte proliferation, and cartilage matrix production in limb skeletons but not in vertebrae.

pathway positively regulates the four cellular processes, and that the Akt-FoxO pathway positively regulates chondrocyte proliferation but negatively regulates chondrocyte maturation and cartilage matrix production. As Akt negatively regulates GSK3, our findings indicated that the Akt-GSK3 pathway negatively regulates chondrocyte maturation, chondrocyte proliferation and cartilage matrix production in limb skeletons but not in vertebrae, at least in part, due to the presence of the proliferating layer, in which GSK3 expression was upregulated, in limb skeletons but not in vertebrae (Fig. 10). These findings indicate that the Akt-mTOR pathway is dominant compared with the Akt-GSK3 and Akt-FoxO pathways in chondrocyte maturation and cartilage matrix production, that the Akt-mTOR and Akt-FoxO pathways are dominant compared with the Akt-GSK3 pathway in chondrocyte proliferation, that the Akt-mTOR pathway is responsible for cell growth of chondrocytes, and that the Akt-GSK3 pathway is involved in skeletal development of limb skeletons but not vertebrae (Fig. 10). Thus, our findings demonstrate that Akt controls the processes of endochondral ossification and skeletal growth by regulating chondrocyte maturation, chondrocyte proliferation and cartilage matrix production through tuning the activities of mTOR, FoxOs, and GSK3 depending on the skeletal part.

In tg(L), chondrocyte maturation and chondrocyte proliferation were enhanced or inhibited depending on the skeletal part, indicating that the Akt activation level or mode affects these processes in a manner dependent on the skeletal part. This may be partly explained by the previous finding that chronic activation of Akt induces feedback inhibition of PI3K activity through both proteasome-dependent degradation of insulin receptor substrate-1 (IRS-1) and inhibition of transcription of IRS-1 as well as that of IRS-2 (Nagoshi et al., 2005). Further, the distribution pattern of GSK3 protein in skeletal elements may also explain the differential regulation of chondrocyte maturation and chondrocyte proliferation in the skeletal parts of tg(L). GSK3 β protein expression was first upregulated in the proliferating layer and further in the hypertrophic chondrocytes in limb skeletons, while it was first upregulated in the hypertrophic chondrocytes in vertebrae, which lack the proliferating layer (Figs. 9C–F). Further, the treatment with lithium chloride severely reduced BrdU uptake in the proliferating layer and severely inhibited chondrocyte maturation in limb skeletons (Figs. 6C, D, G). Thus, the strong inhibition of GSK3 by Akt in myrAkt transgenic mice may result in a decrease of chondrocytes proliferation in the proliferating layer and inhibition of chondrocyte maturation in limb skeletons but not vertebrae. It is also possible that constitutive activation and/or over-activation of Akt affects the cell cycle in a manner different from physiological Akt activation, because chondrocyte proliferation was reduced in *lgl1*-deficient mice but was not enhanced in *Pten* mutant mice (Wang et al., 2006; Ford-Hutchinson et al., 2007). Similar phenomena were observed in the organ culture system. Treatment with lithium chloride or adenoviral introduction of GSK3 β^{S9A} both inhibited chondrocyte proliferation (Fig. 6G, Supplementary Fig. 5G), and treatment with Wnt3a or

adenoviral introduction of dn-Tcf both enhanced chondrocyte proliferation (Figs. 7G, 8J, Supplementary Fig. 5G).

GSK3 is involved in canonical Wnt signaling, hedgehog signaling, and Akt signaling. The function of canonical Wnt signaling in endochondral ossification is complex, because expression of constitutively active β -catenin or deletion of β -catenin in chondrocytes both delayed endochondral ossification (Guo et al., 2004). Further, lithium chloride or SB216763 induced *Fgf18* through the induction of β -catenin, leading to the inhibition of chondrocyte maturation and chondrocyte proliferation (Kapadia et al., 2005). Our findings indicated that canonical Wnt signaling inhibits endochondral ossification, chondrocyte maturation, chondrocyte proliferation, and cartilage matrix production in the physiological condition (Figs. 7C–E, G, 8F–H, J). Hedgehog signaling inhibited endochondral ossification and chondrocyte maturation, enhanced chondrocyte proliferation (Figs. 7C, D, G, 8F, G, J, Supplementary Figs. 5C, D, G) (St-Jacques et al., 1999), and reduced cartilage matrix production (Figs. 7E, 8H). Further, GSK3 inhibited both canonical Wnt signaling and hedgehog signaling (Figs. 7A, B, Supplementary Fig. 5) (Kim and Kimmel, 2006). As treatment with lithium chloride or SB216763 inhibits the kinase activity of GSK3 (Klein and Melton, 1996; Stambolic et al., 1996; Coghlan et al., 2000), resulting in enhancement of the canonical Wnt signaling and hedgehog signaling pathways in addition to inhibition of GSK3 in the Akt-GSK3 pathway, the function of the Akt-GSK3 pathway in the processes of endochondral ossification and skeletal growth remained to be clarified. By blocking both canonical Wnt signaling and hedgehog signaling, however, we unraveled that Akt-GSK3 signaling inhibits endochondral ossification, chondrocyte maturation, chondrocyte proliferation, and cartilage matrix production in limb skeletons but not in vertebrae. Our findings also showed that GSK3 is an important positive regulator for chondrocyte proliferation in the proliferating layer in limb skeletons and exerts its positive effect in a manner independent of hedgehog signaling, because GSK3 inhibits hedgehog signaling (Figs. 6G, 7B, 9C–E). GSK3 upregulation in the proliferating layer in limb skeletons may explain why limb skeletons grow more than vertebrae during development.

Rapamycin inhibited adipogenic differentiation of 3T3-L1 cells and myogenic differentiation of L6A1 cells (Yeh et al., 1995; Coolican et al., 1997; Gagnon et al., 2001), but induced myogenic differentiation of BC3H1 cells and the differentiation of vascular smooth muscle cells (Jayaraman and Marks, 1993; Martin et al., 2007), indicating that mTOR regulates adipogenic or myogenic differentiation positively or negatively depending on the cultured cells and their differentiation stage. Further, the role of mTOR in extracellular matrix production remained to be examined. Our findings clearly showed that the Akt-mTOR pathway positively and dominantly regulates chondrocyte maturation and cartilage matrix production. As mTOR controls protein synthesis through eIF4E and S6K (Hay and Sonenberg, 2004), the increased cartilage matrix production in myrAkt transgenic mice is likely to be due to the enhanced mRNA translation. FoxO1 inhibits adipogenic and myogenic differentiation in vitro (Hribal et al., 2003; Nakae et al., 2003) and FoxO4 represses smooth muscle cell differentiation in vitro (Liu et al., 2005). However, our findings clearly showed that FoxOs promote chondrocyte maturation. Although FoxO3a has been shown to increase the size of cardiac myocytes (Skurk et al., 2005), chondrocyte cell size was not increased by *FoxO3a*-TM nor reduced by dn-FoxO. However, FoxOs promoted extracellular matrix production.

Materials and methods

Generation of transgenic mice

To express the transgene in chondrocytes, cDNA encoding a HA-tagged myrAkt or dominant negative Akt (dn-Akt) (Fujita et al., 2004) was cloned into a vector containing *Col2a1* promoter and enhancer (Ueta et al., 2001). The dominant-negative Akt mutant (dn-Akt) has alanine residues substituted for threonine at position 308 and serine at

position 473. The constitutively active *Akt* (*myrAkt*) has the c-Src myristoylation sequence fused in-frame to the N terminus of the wild-type *Akt* coding sequence that targets the fusion protein to the membrane. An internal ribosomal entry site (IRES) followed by EGFP DNA was inserted into the vector containing *Col2a1* promoter and enhancer at the 3' end of *myrAkt* or *dn-Akt* cDNA (Fig. 1A, Supplementary Fig. 2B). Expression levels of the transgenes were estimated by the relative signal intensity of EGFP and Northern blot analysis. Integration of the transgenes was confirmed by PCR using oligonucleotides, 5'-AGGGCCCCCTCTGCTAACCAT-3' and 5'-CCCTTGCCCAGTAG-TTTCAG-3'. Prior to the study, all experiments were reviewed and approved by Nagasaki University Animal Care and Use Committee.

Skeletal and histological analyses

Alcian blue and Alizarin red staining was performed as described previously (Ueta et al., 2001). Embryos at stages E13.5–18.5, as well as limb and vertebral skeletons from organ culture, were fixed in 4% paraformaldehyde at 4 °C, dehydrated, and embedded in paraffin. Sections (7 µm) were stained with hematoxylin and eosin (HE) or with HE and von Kossa's method. Sections were also stained with safranin O, and extracellular matrix area and chondrocyte cell size were examined using Image J software®. In situ hybridization was performed using mouse *Col2a1* (0.4 kb), mouse *Col10a1* (0.65 kb), mouse *Pthr1* (0.8 kb), mouse *Ihh* (0.6 kb), mouse *Spp1* (1.2 kb), and mouse *aggrecan* (1.5 kb) antisense probes as previously described (Ueta et al., 2001; Yoshida et al., 2004). For monitoring of EGFP signal, embryos were fixed in 4% paraformaldehyde at 4 °C and embedded into O.C.T compound (SAKURA Finetek USA Inc., Torrance, CA), and frozen sections were prepared and analyzed by fluorescent microscopy.

Monitoring of proliferating cells

Mice at E15.5 were injected intraperitoneally with BrdU (50 µg/g body weight) and were sacrificed 1 h later. Femurs and tibiae were fixed in 4% paraformaldehyde in 0.01 M PBS (pH 7.4), and embedded in paraffin. Detection of BrdU-positive cells in the cartilage was performed using anti-BrdU monoclonal antibody (DAKO Japan, Tokyo, Japan). For PCNA staining, sections were reacted with anti-PCNA monoclonal antibody (Progen, Heidelberg, Germany).

Immunohistochemical analyses

Wild-type mice and *myrAkt* transgenic mice at E15.5 or E18.5 were pretreated with Protein Block Serum-Free (DAKO, Japan), and then incubated with goat anti-GFP (Abcam), rabbit anti-type II collagen (Cosmo Bio, LSL, Japan), rabbit anti-Akt, rabbit anti-phosphorylated Akt, rabbit anti-GSK3β, rabbit anti-phosphorylated GSK3β (Cell Signaling Technology, Inc.), rabbit anti-p70 S6K, rabbit anti-phosphorylated p70 S6K (Epitomics, Inc.), rabbit anti-FoxO3a, or rabbit anti-phosphorylated FoxO3a (Upstate) antibody. The localization of the first antibody was visualized by incubation with biotinylated anti-rabbit IgG or anti-goat IgG antibody (Vector Laboratories), and then with peroxidase-conjugated streptavidin (Vector Laboratories). The peroxidase reaction was visualized with diaminobenzidine/hydrogen peroxide solution (DOJINDO, Japan). As negative controls, normal rabbit IgG or goat IgG (IBL) was used instead of the primary antibodies and no significant signals were detected (data not shown).

Cell culture

For micromass culture, limb buds from E12.5 embryos were isolated and were digested in 0.1% trypsin and 0.1% collagenase at 37 °C for 30 min. Then, cells were resuspended in 40 µl drops at 2×10^7 cells/ml, and plated on 12-well plates. After culture for 1 h to allow the attachment of cells, 2 ml of DMEM containing 10% FCS was overlaid.

After culture for 7 days, Alcian blue staining was performed to detect the production of cartilaginous substrates.

Organ culture

Limb and vertebral skeletons were isolated at E15.5 and E16.5, respectively. BGJB medium (GIBCO Co. Ltd., New York, NY) supplemented with 0.25% FCS, 10 mM β-glycerophosphate, 0.6% bovine serum albumin, and 15 µg/ml ascorbic acid was used for the culture, and the medium was changed every day. After cultivation, samples were fixed with 4% paraformaldehyde, and then embedded into paraffin. Forelimbs and the upper half of the spinal column, which were cultured for 4 days, were stained with Alcian blue and Alizarin red, and hind limbs and the lower half of the spinal column, which were cultured for 4 days and 2 days, respectively, were subjected to histological analysis. For BrdU labeling, tibiae were labeled with 10^{-5} M BrdU for 8 h after culture for 2 days and analyzed as described above. We did not observe any deleterious effects on the tissues upon treatment with lithium chloride at concentrations of 10–100 mM, with rapamycin at concentrations of 10–80 nM (data not shown), and with SB216763 at concentrations of 5–20 µM (data not shown).

Adenovirus transfer

FoxO3a triple mutant (*FoxO3a-TM*), *dn-FoxO3a*, and *GSK3β^{S9A}* adenoviruses were gifts from K. Walsh (Skurk et al., 2005), and *Gli*, *dn-Gli* and *Cre* adenoviruses were gifts from R. Nishimura (Osaka University). In *FoxO3a-TM*, the three Akt phosphorylation sites, Thr-32, Ser-253, and Ser-315, were replaced by alanine residues (Brunet et al., 1999). The *dn-FoxO3a* was constructed by deleting the transactivation domain of the C-terminus. In the constitutively active mutant of *GSK3β* (*GSK3β^{S9A}*), the serine residue at position 9 was replaced by alanine. The *dn-Tcf* was constructed by cloning a partial cDNA fragment (amino acids 188–303), which lacks the transactivation domain. *LoxP* sequences were integrated in the *dn-Gli* construct, and the adenovirus expresses *dn-Gli* in the presence of *Cre* recombinase. They were infected at a multiplicity of infection (MOI) of 10 or 20 for 24 h.

Immunoblotting and antibodies

Immunoblot analyses were performed as previously described (Fujita et al., 2004). Proteins were resolved by 10% polyacrylamide gel electrophoresis. The blots were first incubated with rabbit anti-phosphorylated Akt, rabbit monoclonal anti-GSK3β, rabbit anti-phosphorylated GSK3β, rabbit anti-GSK3α, rabbit anti-mTOR, rabbit anti-phosphorylated mTOR (Cell Signaling Tech., Beverly, MA), rabbit anti-p70 S6K, rabbit anti-phosphorylated p70 S6K (Epitomics, Inc.), rabbit anti-FoxO3a, rabbit anti-phosphorylated FoxO3a (Upstate Biotech., Lake Placid, NY), or goat anti-actin (Santa Cruz Biotechnology, Inc., Santa Cruz, CA) antibody, and then with horseradish peroxidase-conjugated anti-rabbit IgG (Cell Signaling Tech.) or anti-goat IgG (Santa Cruz Biotechnology, Inc.) antibody.

Luciferase assay

Reporter assays were performed by transient transfection of 0.1 µg of TOP-flash (Upstate Biotech.) or 8xGli-luc (Sasaki et al., 1997), and 0.002 µg of pRL-CMV using the Dual Luciferase Reporter Assay System (Promega, Madison, WI) as previously described (Fujita et al., 2004). Luciferase activity was normalized to *Renilla* luciferase activity under the control of the CMV promoter.

Statistical analysis

Statistical analyses were performed using Student's *t*-test. A *P*-value of less than 0.05 was considered to be significant.

Acknowledgments

We thank K. Walsh for the *myrAkt* and *dn-Akt* cDNAs and *FoxO3a* and *GSK3 β ^{S9A}* adenoviruses, R. Nishimura for the *Gli*, *dn-Gli*, and *Cre* adenoviruses, H. Sasaki for the 8 \times *Gli* reporter construct, Y. Ito for the Runx2 antibody, M. Iwamoto for the *aggreccan* probe, T. Moriishi for the technical assistance, and A. Kakiya for the secretarial assistance.

Funding: This work was supported by grants from Research Fellowships of the Japan Society for the Promotion of Science and grants from the Japanese Ministry of Education, Culture, Sports, Science and Technology, and the Uehara Memorial Foundation.

Appendix A. Supplementary data

Supplementary data associated with this article can be found, in the online version, at doi:10.1016/j.ydbio.2009.01.009.

References

- Accili, D., Arden, K.C., 2004. FoxOs at the crossroads of cellular metabolism, differentiation, and transformation. *Cell* 117, 421–426.
- Anderson, M.J., Viars, C.S., Czekay, S., Cavenee, W.K., Arden, K.C., 1998. Cloning and characterization of three human forkhead genes that comprise an FKHR-like gene subfamily. *Genomics* 47, 187–199.
- Baker, J., Liu, J.P., Robertson, E.J., Efstratiadis, A., 1993. Role of insulin-like growth factors in embryonic and postnatal growth. *Cell* 75, 73–82.
- Brazil, D.P., Hemmings, B.A., 2001. The years of protein kinase B signaling. A hard Akt to follow. *Trends Biochem. Sci.* 26, 657–664.
- Brodbeck, D., Hill, M.M., Hemmings, B.A., 2001. Two splice variants of protein kinase B gamma have different regulatory capacity depending on the presence or absence of the regulatory phosphorylation site serine 472 in the carboxy-terminal hydrophobic domain. *J. Biol. Chem.* 276, 29550–29558.
- Brunet, A., Bonni, A., Zigmond, M.J., Lin, M.Z., Juo, P., Hu, L.S., Anderson, M.J., Arden, K.C., Blenis, J., Greenberg, M.E., 1999. Akt promotes cell survival by phosphorylating and inhibiting a Forkhead transcription factor. *Cell* 96, 857–868.
- Cantley, L.C., 2002. The phosphoinositide 3-kinase pathway. *Science* 296, 1655–1657.
- Castrillon, D.H., Miao, L., Kollipara, R., Horner, J.W., DePinho, R.A., 2003. Suppression of ovarian follicle activation in mice by the transcription factor Foxo3a. *Science* 301, 215–218.
- Coghlan, M.P., Culbert, A.A., Cross, D.A., Corcoran, S.L., Yates, J.W., Pearce, N.J., Rausch, O.L., Murphy, G.J., Carter, P.S., Roxbee, Cox, L., Mills, D., Brown, M.J., Haigh, D., Ward, R.W., Smith, D.G., Murray, K.J., Reith, A.D., Holder, J.C., 2000. Selective small molecule inhibitors of glycogen synthase kinase-3 modulate glycogen metabolism and gene transcription. *Chem. Biol.* 7, 793–803.
- Cohen, P., Frame, S., 2001. The renaissance of GSK3. *Nat. Rev., Mol. Cell Biol.* 2, 769–776.
- Coolican, S.A., Samuel, D.S., Ewton, D.Z., McWade, F.J., Florini, J.R., 1997. The mitogenic and myogenic actions of insulin-like growth factors utilize distinct signaling pathways. *J. Biol. Chem.* 272, 6653–6662.
- Corradetti, M.N., Guan, K.L., 2006. Upstream of the mammalian target of rapamycin: do all roads pass through mTOR? *Oncogene* 25, 6347–6360.
- Datta, S.R., Brunet, A., Greenberg, M.E., 1999. Cellular survival: a play in three Akts. *Genes Dev.* 13, 2905–2927.
- DeLise, A.M., Fischer, L., Tuan, R.S., 2000. Cellular interactions and signaling in cartilage development. *Osteoarthr. Cartil.* 8, 309–334.
- Ford-Hutchinson, A.F., Ali, Z., Lines, S.E., Hallgrímsson, B., Boyd, S.K., Jirik, F.R., 2007. Inactivation of Pten in osteo-chondrogenitor cells leads to epiphyseal growth plate abnormalities and skeletal overgrowth. *J. Bone Miner. Res.* 22, 1245–1259.
- Frame, S., Cohen, P., 2001. GSK3 takes centre stage more than 20 years after its discovery. *Biochem. J.* 359, 1–16.
- Fujita, T., Azuma, Y., Fukuyama, R., Hattori, Y., Yoshida, C.A., Koide, M., Ogita, K., Komori, T., 2004. Runx2 induces osteoblast and chondrocyte differentiation and enhances their migration by coupling with PI3K-Akt signaling. *J. Cell Biol.* 166, 85–95.
- Furuyama, T., Nakazawa, T., Nakano, I., Mori, N., 2000. Identification of the differential distribution patterns of mRNAs and consensus binding sequences for mouse DAF-16 homologues. *Biochem. J.* 349, 629–634.
- Gagnon, A., Lau, S., Sorisky, A., 2001. Rapamycin-sensitive phase of 3T3-L1 preadipocyte differentiation after clonal expansion. *J. Cell. Physiol.* 189, 14–22.
- Guo, X., Day, T.F., Jiang, X., Garrett-Beal, L., Topol, L., Yang, Y., 2004. Wnt/beta-catenin signaling is sufficient and necessary for synovial joint formation. *Genes Dev.* 18, 2404–2417.
- Hannan, K.M., Brandenburger, Y., Jenkins, A., Sharkey, K., Cavanaugh, A., Rothblum, L., Moss, T., Poortinga, G., McArthur, G.A., Pearson, R.B., Hannan, R.D., 2003. mTOR-dependent regulation of ribosomal gene transcription requires S6K1 and is mediated by phosphorylation of the carboxy-terminal activation domain of the nucleolar transcription factor UBF. *Mol. Cell. Biol.* 23, 8862–8877.
- Hay, N., Sonenberg, N., 2004. Upstream and downstream of mTOR. *Genes Dev.* 18, 1926–1945.
- Hosaka, T., Biggs III, W.H., Tieu, D., Boyer, A.D., Varki, N.M., Cavenee, W.K., Arden, K.C., 2004. Disruption of forkhead transcription factor (FOXO) family members in mice reveals their functional diversification. *Proc. Natl. Acad. Sci. U. S. A.* 101, 2975–2980.
- Hribal, M.L., Nakae, J., Kitamura, T., Shutter, J.R., Accili, D., 2003. Regulation of insulin-like growth factor-dependent myoblast differentiation by Foxo forkhead transcription factors. *J. Cell Biol.* 162, 535–541.
- Jayaraman, T., Marks, A.R., 1993. Rapamycin-FKBP12 blocks proliferation, induces differentiation, and inhibits cdc2 kinase activity in a myogenic cell line. *J. Biol. Chem.* 268, 25385–25388.
- Kandel, E.S., Hay, N., 1999. The regulation and activities of the multifunctional serine/threonine kinase Akt/PKB. *Exp. Cell Res.* 253, 210–229.
- Kapadia, R.M., Guntur, A.R., Reinhold, M.L., Naski, M.C., 2005. Glycogen synthase kinase 3 controls endochondral bone development: contribution of fibroblast growth factor 18. *Dev. Biol.* 285, 496–507.
- Kim, L., Kimmel, A.R., 2006. GSK3 at the edge: regulation of developmental specification and cell polarization. *Curr. Drug Targets* 7, 1411–1419.
- Klein, P.S., Melton, D.A., 1996. A molecular mechanism for the effect of lithium on development. *Proc. Natl. Acad. Sci. U. S. A.* 93, 8455–8459.
- Lawlor, M.A., Alessi, D.R., 2001. PKB/Akt: a key mediator of cell proliferation, survival and insulin response? *J. Cell. Sci.* 114, 2903–2910.
- Le Roith, D., Bondy, C., Yakar, S., Liu, J.L., Butler, A., 2001. The somatomedin hypothesis: 2001. *Endocr. Rev.* 22, 53–74.
- Liu, J.P., Baker, J., Perkins, A.S., Robertson, E.J., Efstratiadis, A., 1993. Mice carrying null mutations of the genes encoding insulin-like growth factor I (Igf-1) and type I IGf receptor (Igf1r). *Cell* 75, 59–72.
- Liu, Z.P., Wang, Z., Yanagisawa, H., Olson, E.N., 2005. Phenotypic modulation of smooth muscle cells through interaction of Foxo4 and myocardin. *Dev. Cell* 9, 261–270.
- Martin, K.A., Merenick, B.L., Ding, M., Fetalvero, K.M., Rzcudlo, E.M., Kozul, C.D., Brown, D.J., Chiu, H.Y., Shyu, M., Drapeau, B.L., Wagner, R.J., Powell, R.J., 2007. Rapamycin promotes vascular smooth muscle cell differentiation through insulin receptor substrate-1/phosphatidylinositol 3-kinase/Akt2 feedback signaling. *J. Biol. Chem.* 282, 36112–36120.
- Nagoshi, T., Matsui, T., Aoyama, T., Leri, A., Anversa, P., Li, L., Ogawa, W., del Monte, F., Gwathmey, J.K., Grazette, L., Hemmings, B.A., Kass, D.A., Champion, H.C., Rosenzweig, A., 2005. PI3K rescues the detrimental effects of chronic Akt activation in the heart during ischemia/reperfusion injury. *J. Clin. Invest.* 115, 2128–2138.
- Nakae, J., Kitamura, T., Kitamura, Y., Biggs III, W.H., Arden, K.C., Accili, D., 2003. The forkhead transcription factor Foxo1 regulates adipocyte differentiation. *Dev. Cell* 4, 119–129.
- Nakashima, K., de Crombrughe, B., 2003. Transcriptional mechanisms in osteoblast differentiation and bone formation. *Trends Genet.* 19, 458–466.
- Peng, X.D., Xu, P.Z., Chen, M.L., Hahn-Windgassen, A., Skeen, J., Jacobs, J., Sundararajan, D., Chen, W.S., Crawford, S.E., Coleman, K.G., Hay, N., 2003. Dwarfism, impaired skin development, skeletal muscle atrophy, delayed bone development, and impeded adipogenesis in mice lacking Akt1 and Akt2. *Genes Dev.* 17, 1352–1365.
- Powell-Braxton, L., Hollingshead, P., Warburton, C., Dowd, M., Pitts-Meek, S., Dalton, D., Gillett, N., Stewart, T.A., 1993. IGF-I is required for normal embryonic growth in mice. *Genes Dev.* 7, 2609–2617.
- Sarbassov, D.D., Guertin, D.A., Ali, S.M., Sabatini, D.M., 2005. Phosphorylation and regulation of Akt/PKB by the rictor-mTOR complex. *Science* 307, 1098–1101.
- Sasaki, H., Hui, C., Nakafuku, M., Kondoh, H., 1997. A binding site for Gli proteins is essential for HNF-3beta floor plate enhancer activity in transgenics and can respond to Shh in vitro. *Development* 124, 1313–1322.
- Skurk, C., Izumiya, Y., Maatz, H., Razeghi, P., Shiojima, I., Sandri, M., Sato, K., Zeng, L., Schiekofer, S., Pimentel, D., Lecker, S., Taegtmeier, H., Goldberg, A.L., Walsh, K., 2005. The FOXO3a transcription factor regulates cardiac myocyte size downstream of AKT signaling. *J. Biol. Chem.* 280, 20814–20823.
- Stambolic, V., Ruel, L., Woodgett, J.R., 1996. Lithium inhibits glycogen synthase kinase-3 activity and mimics wingless signalling in intact cells. *Curr. Biol.* 6, 1664–1668.
- St-Jacques, B., Hammerschmidt, M., McMahon, A.P., 1999. Indian hedgehog signaling regulates proliferation and differentiation of chondrocytes and is essential for bone formation. *Genes Dev.* 13, 2072–2086.
- Ueta, C., Iwamoto, M., Kanatani, N., Yoshida, C.A., Liu, Y., Enomoto-Iwamoto, M., Ohmori, T., Enomoto, H., Nakata, K., Takada, K., Kuru, K., Komori, T., 2001. Skeletal malformations caused by overexpression of Cbfa1 or its dominant negative form in chondrocytes. *J. Cell Biol.* 153, 87–100.
- Wang, Y., Nishida, S., Sakata, T., Elalieh, H.Z., Chang, W., Halloran, B.P., Doty, S.B., Bikle, D.D., 2006. Insulin-like growth factor-I is essential for embryonic bone development. *Endocrinology* 147, 4753–4761.
- Yeh, W.C., Bierer, B.E., McKnight, S.L., 1995. Rapamycin inhibits clonal expansion and adipogenic differentiation of 3T3-L1 cells. *Proc. Natl. Acad. Sci. U. S. A.* 92, 11086–11090.
- Yoshida, C.A., Yamamoto, H., Fujita, T., Furuichi, T., Ito, K., Inoue, K., Yamana, K., Zanma, A., Takada, K., Ito, Y., Komori, T., 2004. Runx2 and Runx3 are essential for chondrocyte maturation, and Runx2 regulates limb growth through induction of Indian hedgehog. *Genes Dev.* 18, 952–963.